Some Applications of the Distorted Wave Approximation for Direct Nuclear Reactions

by

R. H. Bassel

Lectures to be presented at Hercegnovi, Yugoslavia
July 13-29, 1964

Facsimile Price $ 6.10

Microfilm Price $ 2.72

Available from the
Office of Technical Services
Department of Commerce
Washington 25, D. C.

The subject which I will discuss is the distorted-waves theory[1] of direct reactions and its application to the study of nuclei. I shall mainly be concerned with a study of the reaction theory, its range of validity, and its ability to give quantitative information about nuclear structure.

It is necessary to state what is meant by a direct reaction. The definition commonly in use, due to Austern[1], is that a direct reaction involves only a few degrees of freedom of the system, as opposed say to reactions which proceed via a compound nucleus. These few degrees of freedom can be explicitly treated in a reaction calculation while the remaining processes can be completely ignored, in which case we have a plane wave theory, or lumped into a reaction channel which leads, ultimately, to the distorted wave theory.

To make these ideas explicit, it is useful to formally derive the distorted wave matrix element and to show where the various approximations enter in order to do a practical calculation.

The theory will be formulated in a general way, so that rearrangement collisions such as stripping and inelastic scattering appear on the same footing.

Consider the reaction

$$a + A \rightarrow b + B$$

where, say for inelastic scattering,

$b = a$

$B = A^*$ an excited state of the aggregate A,

while for stripping

$$a = d$$

$$b = p$$

$$B = A + n \ .$$

The Hamiltonian for this reaction can be written,

$$H = H_a + H_A + V_{aA} = H_i + V_i \ , \qquad (1)$$

$$= H_b + H_B + V_{bB} = H_f + V_f \ ,$$

where H_a and H_A are the Hamiltonians for the internal motion of aggregates a and A, and V_{aA} is the interaction between them. Similar definitions hold for H_b, H_B, and V_{bB}.

The solution to the non-relativistic Schrodinger equation

$$(H - E)\, \Psi = 0 \qquad (2)$$

is formally straightforward and is easily found using the operator techniques.

If the theory is formulated in the initial system (a, A), the solution of interest has incoming and outgoing waves in the incident channel and only outgoing waves in all other channels. This solution is usually denoted $\Psi_i^{(+)}$, the subscript i referring to incoming and outgoing waves in the incident channel, while the superscript + means only outgoing waves in all other channels.

We proceed by adding and subtracting a potential U_i to the Hamiltaonian, that is rewrite H as

$$H = H_i + (V_i - U_i) + U_i \qquad (1')$$

and define the "distorted" wave $\chi_i^{(+)}$ as the solution of

$$(H_i + U_i - E)\, \chi_i^{(+)} = 0 \quad . \tag{3}$$

If elastic scattering is important U_i is taken as the potential which describes the elastic scattering of a by A and, correspondingly, $\chi_i^{(+)}$ contains the elastic scattered part of the total wave function. $\chi_i^{(+)}$ is written as a product solution

$$\chi_i^{(+)} = \chi^{(+)}(r_{aA})\, \omega_a(\epsilon_a)\, \phi_A(\epsilon_A) = \chi^{(+)}\, \phi_{aA} \tag{4}$$

where $\chi^{(+)}$ describes the relative motion of a and A, and $\phi_a(\epsilon_a)$, $\phi_A(\epsilon_A)$ are wave functions of internal motion of a and A. This product will henceforth be contracted to $\phi_a\, \phi_A = \phi_{aA}$. Then with

$$\Psi_i^{(+)} = \chi_i^{(+)} + \omega_s, \quad . \tag{5}$$

(ω_s, contains all scattered waves other than the elastic wave), application of the Schrodinger equation gives

$$(H - E)\, \omega_s, = -(V_i - U_i)\, \chi_i^{(+)} \quad . \tag{6}$$

Defining the Green's function

$$(H - E)\, G = -1, \; = -\delta(\rho - \rho') \quad , \tag{7}$$

where G is the total Green's function, the solution of the total Hamiltonian with an inhomogeneous point source at $\rho = \rho'$, with ρ representing all the coordinates in the problem, $\vec{\rho} = (\vec{r}, \vec{\epsilon}_a, \vec{\epsilon}_A)$.

Then

$$\varpi_{s'} = G(V_i - U_i)\, \chi_i^{(+)} \tag{8}$$

and integration over the primed coordinates is implied.

Symbolically,

$$G = \frac{1}{E - H + i\epsilon} \tag{9}$$

and the positive continuation ϵ insures outgoing scattered waves.

In the limit $U_i \to 0$, $\chi_i^{(+)} \to \Psi_i$, wherein the relative motion is described by a plane wave, and $\varpi_{s'} \to \varpi_s$ which now contains the elastic scattered parts.

We are interested in that part of $\Psi_i^{(+)}$ in the channel (b, B). To find this note that G can be expanded in eigensolutions of the final system $f \equiv (b, B)$, which we now show. Using the operator relation

$$\frac{1}{A} - \frac{1}{B} = \frac{1}{A}(B - A)\frac{1}{B} \tag{10}$$

we find

$$G = G_f + G_f V_f G \tag{11}$$

where

$$G_f = \frac{1}{E - H_f + i\epsilon} \quad . \tag{12}$$

For our particular final system

$$G_f = -\frac{2M_f}{2\pi\hbar^2} \sum_j G_F^j(r_{bB}, r'_{bB})\, \varphi_{bB}^j(\epsilon_{bB})\, \varphi_{bB}^j(\epsilon'_{bB}) \tag{13}$$

with G^j_F the free Green's function defined by

$$(T - K_j^2)\, G^j_F = -\delta(\vec{r}_{bB} - \vec{r'}_{bB}) , \tag{14}$$

with outgoing solution

$$G^j_F = -\frac{M_f}{2\pi h^2} \frac{e^{i K_j \left|\vec{r}_{bB} - \vec{r'}_{bB}\right|}}{\left|\vec{r}_{bB} - \vec{r'}_{bB}\right|} . \tag{15}$$

Here M_f is the reduced mass of the colliding fragments in the final channel. Since we are interested in the wave function at infinity for a particular final channel f, we project out the bound aggregate φ_{bB} and take the limit as $r_{bB} \to \infty$, that is

$$\lim_{r_{bB} \to \infty} \langle \varphi_{bB} \quad \varphi'_s \rangle = - \frac{e^{i K_f r_{bB}}}{r_{bB}} \langle e^{- i\vec{K}_f \cdot \vec{r}_{bB}} \varphi^*_{bB} (1 + V_f G) \quad (V_i - U_i) \quad \chi_i^{(+)} \rangle . \tag{16}$$

But

$$e^{- i\vec{K}_f \cdot \vec{r}_{bB}} \varphi^*_{bB} (1 + V_f G) = \Psi_f^{+(-)} \tag{17}$$

by a similar analysis.

Here $\Psi_f^{(-)}$ is the solution to the total Hamiltonian with plane wave parts in the final channel but with incoming scattered parts in all other channels. This is necessary to satisfy time reversibility.

A counter at infinity which has been biased to count particles of type b and the proper energy, sees only the spherical wave given by

equation (16), with amplitude

$$f(K_i \to K_f) = -\frac{M_f}{2\pi\hbar^2} \langle \Psi_f^{(-)} \mid V_i - U_i \mid \chi_i^{(+)} \rangle . \tag{18}$$

It is more convenient to work with the T matrix, the element of which is of interest is defined by the relation,

$$f(\vec{K}_i \to \vec{K}_f) = -\frac{M_f}{2\pi\hbar^2} \; T(\vec{K}_i \to \vec{K}_f) . \tag{19}$$

Obviously, the total wave function $\Psi_f^{(-)}$ can be expressed as the sum of a distorted wave and a scattering solution with incoming waves in all channels except f; i.e.,

$$\Psi_f^{(-)} = \left[1 + G^+ (V_f - U_f)^+ \right] \chi_f^{(-)} \tag{20}$$

so that

$$T(\vec{K}_i - \vec{K}_f) = \langle \chi_f^{(-)} \mid V_i - U_i \mid \chi_i^{(+)} \rangle + \langle \chi_f^{(-)} \mid (V_f - U_f)\, G\, (V_i - U_i) \mid \chi_i^{(+)} \rangle . \tag{21}$$

Again from time reversibility

$$T(K_i \to K_f) = T(-K_f \to -K_i)$$

$$= \langle \chi_f^{(-)} \mid (V_f - U_f) \mid \Psi_i^{(+)} \rangle \tag{22}$$

which is apparent from equation (8) for $\Psi_f^{(-)}$. Strictly speaking, this result for the scattering amplitude holds only if the distorting potential is a function only of the relevant relative coordinate.[2]

Although these results are exact, and completely general, the theory has been deliberately formulated to single out the elastic scattering channel which is presumed to be strong. The remaining interaction

$(V_i - U_i)$, or $(V_f - U_f)$ is the residual interaction, that part of the interaction over and above the interaction which gives elastic scattering, and which is responsible for transitions between states. If our assumptions are correct and the reaction amplitude is weak relative to the elastic amplitude, then it is reasonable to treat the reaction in perturbation theory. This amounts to taking

$$T_{exact} \approx T_{DWBA}$$

and setting $\Delta T = \langle \chi_f^{(-)} | (V_f - U_f)\, G\, (V_i - U_i) | \chi_i^{(+)} \rangle$ equal to zero.

The remaining matrix element T_{DWBA} can be written in either the prior form

$$T_{DWBA} = \langle \chi_f^{(-)} | (V_i - U_i) | \chi_i^{(+)} \rangle \qquad (23\text{-}1)$$

or the post form

$$T_{DWBA} = \langle \chi_f^{(-)} | (V_f - U_f) | \chi_i^{(+)} \rangle \ . \qquad (23\text{-}2)$$

The two are formally equivalent, but computationally quite different. The particular choice one uses depends on the physics of the problem.

So we can see that DWBA considers matrix elements of the residual interaction between elastic scattering states. In practice, the relative motion parts of $\chi_i^{(+)}$ and $\chi_f^{(-)}$ are generated from optical potentials which describe the elastic scattering in initial and final channels, (if such data is available). As you know the optical potential is complex, the imaginary part of the potential accounts for the flux taken out of the incident beam and fed into other reaction channels. This flux goes mostly into the compound nucleus channels, but some goes into the direct channels,

including the reaction channel which is being considered explicitly. Similarly, the real part of the optical potential has contributions from the reaction channels which lead to the non-locality of the potential. Thus it is "slightly" inconsistent to use elastic scattering parameters to generate distorted wave functions for reaction calculations. However, it is hoped, and in some cases has been demonstrated, that this causes negligible error.

Remembering that $\chi_i^{(+)}$ and $\chi_f^{(-)}$ are chosen as product solutions, equation (23) is written

$$T_{DWBA} =$$

$$= J \int \vec{dr}_{aA} \int \vec{dr}_{bB}\, \chi^{(-)^+}(\vec{K}_f, \vec{r}_{bB}) \langle b,B|V_{res}| A,a\rangle \chi^{(+)}(\vec{K}_i, \vec{r}_{aA}) \quad (24)$$

with J the Jacobian of the transformation to the relative variables r_{aA}, and r_{bB}.

The matrix element written in this way displays the factorization into a relative motion part consisting of the distorted waves, and a nuclear matrix element

$$\langle b,\ B \left| V_{res} \right| A, a\rangle = \int d\epsilon\ \phi_b^*\ \phi_B^*\ V_{res}\ \omega_a\ \phi_A \quad (25)$$

where the ϵ are the remaining variables independent of the relative coordinates.

This factorization has been much discussed[1] but is worthy of emphasis. The nuclear matrix element contains all the detailed reaction information. It includes the angular momentum selection rules, and its

amplitude yields "directly" the nuclear information sought. Its functional dependence on the channel coordinates r_{aA} and r_{bB} depends on the reaction being studied, differing, for example, for stripping and inelastic scattering. On the other hand, the treatment of the distorted waves, the dynamical part, is much the same for all reactions and leads to computational simplicity.

It is possible to make very general statements about the nuclear matrix element (23). Following Satchler[3], we expand the matrix element into terms where a definite angular momentum J is transferred to nucleus A to form the residual nucleus B.

$$\vec{J} = \vec{J}_B - \vec{J}_A .$$

J is made up of an orbital angular momentum transfer ℓ and a spin part S, where

$$\vec{S} = \vec{S}_a - \vec{S}_b$$

and

$$\vec{\ell} = \vec{J} - \vec{S} .$$

Then

$$J\langle b, B | V_{res} | A, a\rangle = J\langle S_b\, m_b, J_B M_B | V_{res} | J_A\, M_A, S_a\, m_a\rangle$$

$$= \sum_{\ell SJ} (i)^{-\ell} (-)^{S_b - m_b} G_{\ell SJ, m}(\vec{r}_{aA}, \vec{r}_{bB}; bB, aA) \quad x$$

$$\langle J_A\, J\, M_A, M_B - M_A | J_B\, M_B\rangle \langle S_a\, S_b\, m_a - m_b | S\, m_a - m_b\rangle$$

$$\langle \ell S m, m_a - m_b | J\, M_B - M_A\rangle \qquad (26)$$

where the Clebsch-Gordan coefficients take care of the angular momentum coupling, and $m = M_B + m_b + M_A - m_a$.

By inversion

$$G_{\ell SJ,m} = J \sum_{\substack{M_A, M_B \\ m_a, m_b}} (i)^{\ell} \left(\frac{2\ell+1}{2J_B+1}\right) \langle S_b m_b, J_B M_B \,|\, V_{res} \,|\, J_A M_A, S_a M_a \rangle \times$$

$$(-)^{S_b - m_b} \langle J_A J M_A, M_B - M_A \,|\, J_B M_B \rangle \times$$

$$\langle S_a S_b m_a - m_b \,|\, S m_a - m_b \rangle \langle \ell S m, m_a - m_b \,|\, J M_A - M_B \rangle. \qquad (27)$$

The possible dependence of $G_{\ell SJ,m}$ on the nuclear and projectile quantum numbers is denoted by the appearance of B, b, and A, a as arguments of this function. From the form of G it is seen to have angular momentum properties like Y_{ℓ}^{*m}. It also carries the parity of the transition, $\pi(a)\pi(A)\,\pi(b)\pi(B)$ through the matrix element (23).

In general the function G can be factored into an amplitude and a form factor,

$$G_{\ell SJ,m} = A_{\ell SJ,m}\, f_{\ell SJ,m}(\vec{r}_{aA}, \vec{r}_{bB}) . \qquad (28)$$

where A is often chosen to include spectroscopic information (e. g. fractional parentage coefficients) and the interaction strengths.

This factorization, while not necessary, is convenient, so that one can study standard form factors and incorporate the normalization at the end. For example, in the study of neutron hole states, by say the (p, d) reaction or by the (^{3}He, α) reaction, the form factor will be the same but the amplitude, $A_{\ell SJ,m}$, different.

Going back to equation (24), the total amplitude may be rewritten

$$T_{DWBA} = \sum (2J+1)^{1/2} \langle J_A\, J\, M_A,\ M_B - M_A \mid J_B M_B \rangle B_{SJ}^{\ell m\, m_b m_a}(\vec{K}_f, \vec{K}_i) \quad (29)$$

with

$$B_{SJ}^{\ell m\, m_b m_a} = \frac{(i)^{\ell}}{(2J+1)^{1/2}} \sum_{m'_a m'_b m} \langle \ell S m',\ m'_a - m'_b \mid J m - m_b + m_a \rangle$$

$$\langle S_a S_b m'_a - m'_b \mid S\, m'_a - m'_b \rangle\, (-)^{S_b - m_b} J \int d\vec{r}_{aA} \int d\vec{r}_{bB}$$

$$\chi^{(+)-}(\vec{K}_f,\ \vec{r}_{bB})\, f_{\ell SJ,m}(r_{aA},\ r_{bB})\, \chi^{(+)}(K_i,\ r_{aA}) \ . \quad (30)$$

In terms of which the differential cross section for unpolarized projectiles and targets becomes

$$\frac{d\sigma}{d\Omega} = \frac{M_a M_b}{(2\pi\hbar^2)^2} \frac{K_f}{K_i} \frac{2J_B + 1}{(2J_A + 1)(2S_a + 1)} \sum_{J\, m\, m_b m_a} \Big| \sum_{\ell SJ} A_{\ell SJ}\, B_{SJ}^{\ell m\, m_a m_b} \Big|^2 . \quad (31)$$

In (31) the sum over ℓ, the orbital angular momentum transfer, and S, the spin transfer is coherent, but the sum over J is incoherent. That is different values of ℓ and S leading to the same J can interfere, but different J's cannot. If the amplitude depends only on m_a and m_b through the angular momentum coupling coefficient, that is if the overlap integral involving the distorted waves is not dependent on these quantum numbers, these sums can be performed and the cross section becomes incoherent in ℓSJ and m.

To complete our treatment of the general theory, we must discuss the properties of the distorted waves $\chi^{(+)}$ and $\chi^{(-)}$.

As we have stated, the distorted wave theory generally assumes the elastic scattering to be strong and attempts to take this into account "exactly".

In practice this means generating these functions from the Schrödinger equation with the optical potential which explains the elastic scattering.

The local optical potentials currently in vogue have forms for the real potential which are constant for small separations of the colliding fragments and fall smoothly to zero for large separations. The most popular shape is the Woods-Saxon form

$$V(r) = - V_o/(1 + e^x)$$

$$x = (r - r_o A^{1/3})/a \qquad (32)$$

with $r_o A^{1/3}$ the "nuclear" radius and 4.4a the skin thickness.

The absorbtive potential can have this same form, or be surface peaked or a mixture of the two, e.g.

$$W(r) = - W_o/(1 + e^{x'}) - 4W_D\, e^{x'}/(1 + e^{x'})^2 \qquad (33)$$

with

$$x' = (r - r_W A^{1/3})/a_W \ .$$

If the particles are charged, the potential includes a Coulomb interaction, which, for a point charge incident on a uniform charge distribution with radius R_c, is

$$U_c = \frac{Z\, Z'\, e^2}{r} \qquad r \geq R_c$$

$$= \frac{Z\,Z'\,e^2}{2R_c}\,(3 - r^2/R_c^2) \quad r \le R_c \quad . \tag{34}$$

For scattering in which projectile and target have finite charge distributions, the Coulomb interaction can be simulated with this form with a judicious choice of the charge radius parameter R_c.

Finally for particles with spin, a spin-orbit interaction of the form

$$V_{so} = \left(\frac{\hbar}{M_\pi C}\right)^2 \frac{V_s}{ra} \frac{d}{dx}(1 + e^x)^{-1}\,(\sigma \cdot L) \tag{35}$$

is added.

Neglecting, for the time being spin orbit coupling in the optical potentials, the distorted waves can be expanded as

$$\chi^{(+)}(\vec{K}_i, \vec{r}_{aA}) = \frac{4\pi}{K_i\, r_{aA}} \sum_{L_A M} i^{L_A}\, \chi_{L_A}(K_i, r_{aA})\, Y^{*M}_{L_A}(\hat{K}_i)\, Y^{M}_{L_A}(\hat{r}_{aA}) \tag{36}$$

with the χ_{L_A} the solutions of the Schrödinger equation

$$\left\{\frac{d^2}{dr_{aA}^2} + K_i^2 - L_A(L_A + 1)/r_{aA}^2 - \frac{2M}{h^2}\left[V(r) + iW(r) + U_c(r)\right]\right\}\chi_L = 0 \; . \tag{37}$$

Asymptotically, where the nuclear potentials have vanished, the partial waves solutions have the form

$$\chi_{L_A} = \frac{i}{2}\left[H^*_{L_A}(K_i, r_{aA}) - \eta_{L_A} H_{L_A}(K_i, r_{aA})\right] e^{i\sigma_{LA}} \tag{38}$$

where $H_L = (G_L + i\,F_L)$, the Coulomb functions irregular and regular at the origin and σ_L is the Coulomb phase shift, and η_L is the reflection coefficient for the L'th partial wave.

The time reversed solution $\chi^{(-)}(\vec{K}_f, \vec{r}_{bB})$ satisfies ingoing boundary conditions and is the solution of the Schrodinger equation with the complex conjugate of the potential. However, $\chi^{+(-)}$ is the solution of interest and is related to the outgoing solution by

$$\chi^{+(-)}(\vec{K}_f, \vec{r}_{bB}) = \chi^{(+)}(-\vec{K}_f, \vec{r}_{bB}) \tag{39}$$

and is expanded accordingly.

Except for the trivial case of zero nuclear potentials, the Schrodinger equation must be solved numerically for each of the partial wave solutions χ_{L_A}, χ_{L_B}. The distorted wave matrix element is then seen to be a six-dimensional integral, which is in general a rather complicated and difficult calculation. To bypass this difficulty, the zero-range approximation is often introduced, and the six dimensional integral is reduced to a much more manageable three-dimensional integral. In this approximation particle b is assumed to be produced at the point that particle a is absorbed, that is $f_{\ell SJ,m}(\vec{r}_{aA}, \vec{r}_{bB}) \rightarrow \delta(\vec{r}_{bB} - \frac{M_A}{M_B}\vec{r}_{aA})$ $f_{\ell SJ,m}(\vec{r}_{aA})$. The merits of this approximation depend on the reaction. For inelastic scattering without exchange, and if the interaction is local, the zero range approximation is exact. For other reactions Austern et al.[4] have suggested the validity of the zero-range approximation can be assessed by transforming the matrix element (22) into momentum space, separately Fourier analyzing the product of the distorted waves and the form factor $f_{\ell SJ,m}$. If only the small momentum components of the distorted waves are important, such as found in surface reactions, then only the small momentum components of the form factor will contribute and zero-range approximation will be quite good.

Taking this approximation, we are able to handle the angular momentum variables of the matrix elements exactly. With the expansion (24) for the relative motion parts ($\chi^{+(-)}$, $\chi^{(+)}$) and remembering $f_{\ell SJ,m}$ behaves as Y_{ℓ}^{*m}, the reduced amplitude $B_{SJ}^{\ell m\, m_a m_b}$ becomes (in the case of no spin orbit),

$$B_{SJ}^{\ell m\, m_a m_b} = (-)^{S_b - m_b} \left(\frac{2\ell + 1}{2J + 1}\right) \langle \ell s m, m_a - m_b \,|\, J\, m + m_a - m_b \rangle \quad x$$

$$\langle S_a S_b\, m_a, -m_b \quad S\, m_a - m_b \rangle \sum_{L_A L_B} \Gamma_{L_B L_A}^{\ell m} \; P_{L_B}^{m} \; f_{L_B L_A}^{\ell sj} \qquad (40)$$

with

$$\Gamma_{L_B L_A}^{\ell m} = (i)^{L_A - L_B - \ell} (2\, L_B + 1)^2 \left[(L_B - m)! / (L_B + m)!\right]^{1/2} \quad x$$

$$\langle L_B\, \ell\, 0, 0 \,|\, L_A\, 0 \rangle \langle L_B\, \ell\, m - m \,|\, L_A\, 0 \rangle \qquad (41)$$

and

$$f_{L_B L_A}^{\ell sj} = \frac{(2\pi)^{1/2}}{K_i K_f} \frac{M_B}{M_A} \int \chi_{L_B} \left(K_f, \frac{M_A}{M_B} r\right) f_{\ell sj}(r)\, \chi_{L_A}(K_i, r)\, dr \qquad (42)$$

are the radial integrals which must, in most cases, be evaluated numerically.

An important property carried by the Γ coefficient is that the parity change in the reaction $(-)^{L_A + L_B}$ is equal to $(-)^{\ell}$ through the Clebsch-Gordan coefficient $\langle L_B\, \ell\, 0, 0 \,|\, L_A\, 0 \rangle$ which vanishes unless the sum of the angular momenta $L_A + L_B + \ell$ is even.

Let us pass on to the study of single nucleon stripping or pickup which has been the subject of intensive investigation. In particular we shall specialize to deuteron stripping, which, if we ignore the D-state of the

deuteron and tensor forces, is the simplest and best understood example of a nuclear re-arrangement collision.

The coordinate system for the reaction is shown in Fig. 1. In terms of our previous notation

$$\vec{r}_{aA} \to \vec{r}_{d}$$

$$\vec{r}_{bB} \to \vec{r}_{pB}$$

$$L_A \to L_D$$

$$L_B \to L_p \quad .$$

The proton is considered elementary and for these purposes has no internal structure, therefore

$$\varphi_b(\epsilon_b) = \Psi_{1/2, m_b}(\sigma_b), \tag{43}$$

the normalized spin function. The deuteron is an S state of relative motion and may be described say, by the product of the Hulthen wave function

$$\varphi_d(r_{np}) = N\left(\frac{e^{-\alpha r_{np}} - e^{-\beta r_{np}}}{r_{np}}\right) \tag{44}$$

and the spin function

$$\Psi_{1, m_a}(\sigma_a) \quad . \tag{44'}$$

Here $\alpha = \sqrt{\frac{M \epsilon_d}{\hbar^2}}$, with ϵ_d the binding energy of the deuteron, and M is the nucleon mass. The current value of β is 7α.

The nuclear wave function Φ_B may be expanded into a fractional parentage expansion, over the eigenstates of the target nucleus A, as discussed by McFarlane and French[4], i.e.,

$$\Phi_B^{J_B M_B}(r_n, S_n, \epsilon_A) = \sum_{\ell J s m} \Phi_{jm}^{J'_A M'_A}(\epsilon_A) (n I_{\ell sj})^{1/2} U_{\ell sj}(r_n) Y_\ell^{*m}(\hat{r}_n) \quad x$$

$$\Psi_{s, m_s}(\sigma_n) \langle J'_A J M'_A, M_B - M_A \mid J_B M_B \rangle \langle \ell s m, m_s \mid J M'_A - M_B \rangle . \quad (45)$$

Where the Clebsch-Gordan expresses the coupling of J to J'_A to form the nucleus B with angular momentum J_B, $U_{\ell sj}(r_n)$ is the radial wave function of the captured neutron and $\Psi_{s, m_s}(\sigma_n)$ is the spin wave function of the neutron.

$I_{\ell sj}$ is the coefficient of fractional parentage, and n is the number of equivalent nucleons in the orbit into which the nucleon is captured.

The spectroscopic amplitude $S_{\ell sj}$ defined by French[5] and McFarlane[4] and French[5] is related to these numbers by

$$S_{\ell sj} = n (I_{\ell sj})^2 \quad (46)$$

and is a measure of the probability that the final nucleus is made up of the configuration of the initial nucleus and the captured nucleon, and is normalized to n if there are n particles outside an inert core.

The precise determination of S is the object of stripping experiments and theories, for it is this number which yields information about the structure of the nucleus. Once extracted from the data it can be compared with the predictions of a nuclear model.

For the (d, p) problem, the initial interaction is

$$V_i = V_{dA} \equiv V_{nA} + V_{pA} \tag{47}$$

and the final interaction is

$$V_f = V_{pB} \equiv V_{np} + V_{pA} \ . \tag{48}$$

Of the matrix elements (21) the post form is chosen, and the residual interaction

$$V_{res} = V_f - U_f = V_{np} + V_{pa} - U_{pB} \tag{49}$$

is approximated as

$$V_{res} = V_{np} \tag{50}$$

on the basis that there is cancellation between the proton-target interaction and the optical potential in the final channel. This cancellation is certainly not complete, in particular the non-diagonal terms of V_{pA} correspond to target excitation. Additionally, V_{pA} is considered to be the sum of two body interactions; it is real while V_{pA} is complex. Thus our choice of the neutron-proton interaction is based on the idea that it is the dominant part of the interaction for stripping, and can be viewed as a model to be affirmed or refuted by experiment. Lack of success may then be attributed to our neglect of the other terms, as well as the higher order processes neglected.

This choice of V_{np} as the interaction and the method of expanding the nuclear wave functions to separate off one particle indicate that the stripping reaction only gives information about single particle states of

nuclei. The role of the other nucleons is contained in the neglected parts of the amplitude and in the treatment of the distorted waves.

Thus the nuclear matrix element after the required integrations is

$$\langle b,\ B \left| V_{res} \right| A,\ a \rangle = \sum_{\ell s J} (-)^{s_b - m_b} \langle J_A\ J\ M_A,\ M_B - M_A \left| J_B - M_B \right. \rangle$$

$$\langle \ell s m\ m_a - m_b \left| \right. J\ M_B - M_A \rangle \langle S_a\ S_b\ m_a - m_b \left| \right. S\ m_a - m_b \rangle$$

$$\frac{\sqrt{2S_a + 1}}{2S + 1} (n I_{\ell s j})^{1/2} U_{\ell s j}(r_n)\ Y_\ell^{*m}\ V_{np}\ \varphi_d(r_{np}) \qquad (51)$$

which by comparison with equation (26) yields

$$G_{\ell S J, m} = \frac{\sqrt{2S_a + 1}}{2S + 1} (n I_{\ell s j})^{1/2} U_{\ell s j}(r_n)\ Y_\ell^{*m}\ V_{np}\ \varphi_d(r_{np}). \qquad (52)$$

We take the zero range approximation by writing

$$V_{np}\ \varphi_d(r_{np}) = D_o\ \delta(r_{np}) \qquad (53)$$

where

$$D_o = \int V_{np}\ \varphi_d(r)\ \vec{dr}$$

$$= -\frac{\hbar^2}{m} \int (\nabla^2 - a^2)\ \varphi_d(r)\ .$$

Wtih the Hulthen wave function this integral is evaluated to be

$$D_o = -\frac{\sqrt{8\pi}\ |\epsilon_d|}{a^{3/2}} \left(\frac{a + \beta}{\beta}\right)^{3/2}$$

$$\approx \sqrt{1.5} \times 10^2\ \text{MeV}\ f^{3/2}\ . \qquad (54)$$

From equation (28) we choose

$$A_{\ell S J, m} = \sqrt{\frac{2S_a + 1}{2S + 1}} (n I_{\ell s j})^{1/2} D_o$$

and $f_{\ell sj}(r) = U_{\ell sj}(r)$, the neutron bound state radial wave function.

In the calculations on which I shall report the single particle wave functions $U_{\ell sj}(r)$ are normalized eigensolutions of the Schrodinger equation with a well of the Woods-Saxon shape. The well used has two parameters, the radius r_o and diffusivity a. These parameters are not well known and in practice are usually taken the same as the optical parameters for the proton scattering. The depth is adjusted until an eigenstate of the proper energy is found. The functions so generated are similar to oscillator functions in the interior and asymptotically are Hankel functions.

Armed with this apparatus, how good is the theory? A good theory is required to reproduce at least two things, the shape of the angular distribution and the absolute magnitude. For surface reactions the shape of the differential cross section is not too dependent on the shape of the form factor f (equivalently, the nuclear matrix element), but the absolute magnitude is. The shape of the angular distribution is dependent on the angular momentum transfer, and the distorted waves. Often it is possible to find good agreement with the differential cross-section shape, but poor agreement in magnitude. This is taken as a failure of the theory.

There have been many distorted wave analyses of stripping reactions, mostly for nuclei for which the spectroscopic amplitude is not well known, and for which elastic scattering data in either entrance or exit channels were not available. Most of these analyses give quite reasonable fits, but at the expense of arbitrarily varying the parameters of the optical model. It is important to gauge the theory by studying a case in which the elastic scattering data is available, as well as the reaction data and for which a reasonable estimate of the spectroscopic

amplitude is available a priori. Recent measurements by Lee, Schiffer, and Zeidmann at Argonne provide such data[7]. In their experiments they have measured the elastic scattering of deuterons from ^{40}Ca, and the stripping of neutrons to form states in ^{41}Ca. Since ^{40}Ca is doubly magic, these states in ^{41}Ca are assumed to be states of a single neutron coupled to an inert core. Thus the spectroscopic amplitude should be unity. There is some evidence in this data that this is not completely correct. There are two $P_{3/2}$ states at 2 MeV and 2.5 MeV excitation. Also the MIT group has found several $\ell = 1$ groups at higher excitations.

Other appealing reasons for the study of these reactions are: (1) calcium is sufficiently heavy so that the difficulties associated with optical model analyses of scattering from light nuclei might not appear, and (2) these experiments have been done at deuteron bombarding energies of 7, 8, 9, 10, 11, and 12 MeV, allowing a study of the energy dependence.

There is some information lacking, namely the elastic data of proton scattering from ^{41}Ca, which cannot be measured. To bypass this difficulty, use can be made of the systematics of the proton parameters found by Perey[8]. Alternatively, there is data available for the scattering of protons from argon-40 from 8 to 14 MeV which has been fitted[9] and later applied to the scattering of protons from ^{42}Ca with equally good results. Samples of these fits are shown in Fig. 2. The parameters are similar to the Perey parameters except for a smaller real radius parameter. The analysis I shall discuss makes use of the fitted parameters.

The deuteron elastic scattering data was analyzed at the appropriate energies[7]. The optical potentials are a function of the relative coordinate measured from the center-of-mass of the deuteron.

Asymptotically this is correct, aside from small Coulomb effects, but close to the nucleus it is probably in serious error. Here the deuteron can break up, which for scattering is compensated for by the imaginary potential. Thus the wave functions in the interior are in serious doubt, but the error caused in distorted wave calculations must be assessed by comparison with experiment.

As is known from the work of Halbert and Perey and Perey[10], the deuteron optical potentials are characterized by a small real parameter and a surface imaginary potential peaked at a radius somewhat larger than the real radius. The potentials found in this work are of the same form, differing however in having a smaller strength and a larger radius for the imaginary well.

Unfortunately, the elastic scattering can be fitted with a multitude of potentials, all of which give essentially the same phase shifts, and therefore the same scattering. The reasons for this are understood[11]. Briefly, it follows from the fact, shown by Austern[12], that for strongly absorbed particles, the low partial waves can be treated in WKB approximation. Austern demonstrates that the reflection coefficient can be written as the sum of two parts. One arising from the reflection from the nuclear surface, affecting the higher partial waves which are weakly attenuated, the other arising from reflection from the angular momentum barrier in the interior of the potential. Thus, the nuclear volume influences the angular distribution through the low partial waves that are not too attenuated. Neglecting reflection from the surface the

reflection coefficient for the ℓ'th partial wave can be written

$$\eta_\ell = \exp\left[2i\, S_\ell(r_\ell)\right] \tag{55}$$

with

$$S_\ell(r_\ell) = C_\ell + \int_{r_\ell}^{\infty} \left[K_\ell(r)\, dr\right]$$

and r_ℓ the classical turning point. Here $K_\ell(r)$ is the local momentum in the well and is given by

$$K_\ell^{\,2}(r) = \frac{2M}{\hbar^2}\left[E_{cm} - V(r) - V_c(r) - i\,W(r) - \frac{\hbar^2}{2Mr^2}\,\ell(\ell+1)\right] \tag{56}$$

and C_ℓ is a constant independent of the potentials.

If now V and W are replaced by V' and W' so that

$$S_\ell(r'_\ell) = S_\ell(r) \pm n\pi, \quad n = 1, 2, 3.....$$

it follows that this contribution to η_ℓ is unchanged. Physically this means we can add an integer number of half wave lengths on the interior without changing the asymptotic behavior of the wave function, for those partial waves for which reflection from the surface is negligible.

(Optical potentials for protons and neutrons do not show these ambiguities, except for isolated cases, because nucleons are not strongly absorbed. In any case, since the optical potential is the positive energy continuation of the shell model potential, a choice can be made.)

It turns out that there are potentials with real well depths from 30 to 450 MeV, see Table I, and deeper ones could be found. The scattering given by several of these wells for 11 MeV deuterons is shown in Fig. 3.

Except for X the scattering is the same for all potentials and comparison of $S_\ell(r_\ell)$ for low partial waves given by these potentials show that they indeed differ by almost π.

It is interesting to look at the wave functions generated by potentials as they enter directly into the stripping problem. Figure 4 shows the total wave functions plotted along the beam axis for potentials X, Y, and Z. The additional multiples of a wavelength added in the interior change the wave function inside while asymptotically they are much the same. Clearly they will give much different results for the stripping unless the interior contribution is eliminated. This is illustrated in Fig. 5, which shows the distorted wave cross sections for the ground state transfer, with the various deuteron wave functions. The radial integrations are done from the origin to infinity. The data of Lee et al.[7] is also shown. Potential X is clearly unsatisfactory, and Y is little better. The remaining potentials adequately reproduce the peak position but require different spectroscopic factors. G and J especially underestimate the cross section and require a spectroscopic amplitude greater than 1. The same kind of calculations were carried out for the first excited state which is $P_{3/2}$ and the results are shown in Fig. 6. Here the situation is much better, all potentials give the correct peak position and with strengths which do not exceed unity. The deeper potentials, especially Z, are to be preferred because they give better agreement with the large angle data.

These curves exhibit the dependence of the calculations on the interior contributions. For potential X, the wave function is fairly broad

inside, while for G and J the wave functions are rapidly oscillating and have small contributions from the interior. For the capture of the neutron into the 1f orbit, these contributions are fairly important. For capture into the 2p orbit, they are less important because the bound state function has a node on the interior. Since the wave function changes sign there is cancellation in the interior and consequently the surface dominates, where the deuteron wave functions are similar. Of course, if the radial integrals are carried out from some lower cutoff radius where the relative wave functions are the same, the results for all potentials are identical, as shown in Fig. 7.

This multiplicity of potentials forces a choice as to which potential is most physically meaningful, if any. The arguments against the validity of the deuteron wave functions might imply that any of these with a suitable cutoff radius on the integrals might suffice. However, this gives results for the ground state for which the magnitude is too small, comparable to the predictions of G and J in Fig. 5. On the basis of Figs. 5 and 6, the shallow potentials are discarded because of poor fits, the deeper potentials because of the large magnitude necessary for agreement with experiment. This leaves potential Z which has a depth of about 100 MeV, and which incidentally gives the best agreement in shape. We might have argued that we should have chosen a potential of this depth a priori, on grounds that the deuteron optical well is in some sense the superposition of the neutron and proton optical wells averaged over the internal motion of the deuteron. This then implies that the very deep wells are unphysical and suggests a well depth of about 100 MeV (or shallower!).

Figures 8 through 11 show the results of the distorted wave calculations for stripping to the ground state, and the first three excited states. The solid curves are calculated without a cutoff and the dashed curves for a radial cutoff of 4 fermis. These calculations were made with deuteron potentials which give the best fit to elastic scattering at the energies measured. The linear plots serve to emphasize the small angle data, although it is apparent that the detailed fits to large angles is not very good. Some of this large angle discrepancy may be attributed to the theory, but the data show marked changes as a function of energy, especially the second peak in the ground state angular distributions. For the most part there is little necessity for a radial cutoff. The spectroscopic amplitudes found as a function of energy from normalizing the theory to the main peak are listed in Table II. With the best fit potentials they show marked variations due to fluctuations in the elastic data. By using an average deuteron potential which gives reasonable fits to the elastic data, the energy variation of the spectroscopic factors is smoother. From this table note that the $f_{7/2}$ and $p_{1/2}$ strengths are somewhat less than one, while the full $p_{3/2}$ strength is contained in the two levels measured. As was mentioned there are p states at higher excitation whose J is unknown, tentatively they may be assigned as $p_{1/2}$ and could supply some of the remaining $p_{1/2}$ strength. Note that the radial cutoff makes the spectroscopic factor greater than one. The errors associated with these numbers arise from uncertainties and fluctuations in the stripping data, as well as the analyses. The fact that the $f_{7/2}$ strength is less than unity is probably due to uncertainties in these analyses and in the data, although it may reflect a property of ^{41}Ca.

The energy variation is shown on the next figure (12), where the peak cross section is plotted as a function of energy. The black dots are experiment , the open triangles are the calculations using the best fits to the elastic data, while the line represents the average deuteron potential. Except for the 11 MeV points where the measured cross section for the ground state suddenly rises, the average potential gives quite good agreement with the data.

To point out the necessity of having some idea of the elastic scattering, calculations were performed using deuteron potentials recommended by Perey and Perey[10] and by Hodson[13]. The predictions these potentials give for the elastic scattering are shown in Fig. 13, labelled PB and H, and are poor compared to the fit found with the Z-potential. On the other hand, these potentials are quite adequate in predicting the stripping angular distribution shape, Fig. 14, but again poor in absolute magnitude. From this study we conclude that a knowledge of the elastic data is essential if quantitative spectroscopic information is the goal of the investigation. On the other hand our previous remarks suggest that too close attention to the data can also be misleading. Fluctuations in the elastic data gives parameter fluctuations which are reflected in the spectroscopic factors.

It would seem that ideally measurements should be made in a smooth portion of the excitation curve, or experiments performed over a small energy range so that an average can be obtained. Less pessimistically, if there is scattering data available from neighboring nuclei taken at energies close to that of the stripping experiment, this information will be sufficient to extract meaningful spectroscopic information.

This then is an exhaustive study of the zero-range approximation for stripping. The analyses give fair agreement with the data, yielding spectroscopic factors within 80% of what would be expected on a simple model of the ^{41}Ca nucleus. The situation is not wholly satisfactory; there are still discrepancies in fit at large angles which are more clearly seen in a logarithmic plot such as Fig. 14, which shows the 12 MeV data with the calculations using the Z-potential.

These discrepancies might arise from a number of sources. For example, the neglected interactions, higher order terms, spin effects, and spurious contributions from the interior.

Let us first consider the interior contributions and how to modify the theory to take better account of them. The simplest procedure is to introduce a radial cutoff on the radial integrals. Examination of Figs. 8-11 and Fig. 15 shows that this sometimes qualitatively improves the fit, but at the same time overestimates the spectroscopic factors.

Nevertheless, we do not believe in the contributions from the interior and seek better methods than a cutoff to eliminate them.

There are several corrections which do this in a natural way. The first of these is to relax the zero-range approximation and allow the neutron-proton force to have a finite range. This means that we consider both variables r_d and r_p. To accomplish this the form factor $f_{\ell SJ,m}(\vec{r}_d, \vec{r}_p)$ can be expanded in multipoles of both arguments (Satchler[3])

$$f_{\ell SJ,m}(\vec{r}_d, \vec{r}_p) = \sum_{L_1 L_2} F^{sj}_{\ell L_1 L_2}(r_d, r_p)\, Y^{*m}_{L_1}(\theta_d, \varphi_d) \qquad x$$

$$Y_{L_2}^{M-m^*}(\theta_p, \varphi_p)\, \langle L_1\, L_2\, M,\, m-m \,|\, \ell m \rangle \qquad (57)$$

where the Clebsch-Gordan coefficient ensures that the original f behaves like the spherical harmonic $Y_\ell^{m^*}$.

The angular integrations can then be done, yielding $L_1 = L_d$, and $L_2 = L_p$. The remaining problem is then to compute the Kernal functions $F^{sj}_{\ell L_p L_d}(r_d, r_p)$ which is by no means a trivial task. The derivation is quite lengthy and full details are given in the paper of Austern et al. For our purposes it is sufficient to say that it is do-able. It turns out that for stripping, since the deuteron is an internal S-state of motion, that the angular momentum algebra described in zero-range can be carried over to the finite range case. A flexible code has been constructed by Drisko and Satchler and the effects of finite range can be calculated

Some qualitative features are easily discussed. For stripping consider the product $V_{np}\varphi_d$, which previously was set equal to a delta function to go to the zero-range approximation. Now we take

$$V_{np}(r_{np})\, \varphi_d(r_{np}) = \frac{\hbar^2}{m}(\nabla^2 - \alpha^2)\, \varphi_d \qquad (58)$$

and for the Hulthen function takes the Yukawa form

$$V_{np}(r_{np})\, \varphi_d(r_{np}) = N(\alpha^2 - \beta^2)\, \frac{e^{-\beta r}}{r}\,. \qquad (59)$$

The Fourier transform of this function is

$$G(K) = D_o\, \frac{\beta^2}{\beta^2 + K^2} \qquad (60)$$

with D_o as before. The zero-range approximation is taken as $K = 0$.

This function is peaked at K = 0 and falls off with increasing K. On the surface where the potentials are weak

$$Kd = \left[\frac{2Md}{\hbar^2}(V_d - E)\right]^{1/2} \tag{61}$$

and

$$Kp = \left[\frac{2Mp}{\hbar^2}(V_p - E)\right]^{1/2} \tag{62}$$

approach their asymptotic values. There the momentum transfer $(1/2\ \vec{Kd} - \vec{Kp})$ is small for medium energy projectiles, and therefore only the small momentum components of G(K) are sampled. This indicates that for reactions confined to the surface the zero-range approximation will be good. In the interior where the local momenta are large, there will be a net suppression over the zero-range approximation. However, small momentum transfer components are still present in the interior which allows small momentum transfers to be important even at large scattering angles.

(As an aside, if only low momentum components turn out to be important, the range function of the Yukawa form can be replaced by a Gaussian with a range and normalization chosen to match the Yukawa form for small values of the momentum variable. This is attractive for computational purposes, because of the simple expansion properties of the Gaussian.)

The effects of the finite range correction are illustrated in Fig. 16, which compares the zero-range approximation, with and without a cutoff, to the finite range calculations without a cutoff, for the ground state transition at a deuteron energy of 11 MeV. Two sets of

curves are shown, computed with the Z potential and the Y potential. To be noted is that the finite range effects are bigger for the shallower potential because the wave function for the shallower potential is less oscillatory in the interior than for the deep potential. The overall effect is to uniformly decrease the overall magnitude of the curves without appreciably changing the shape, arising from the dominance of small momentum transfers.

On the plane wave Born approximation, the finite range effects are more drastic. There the zero-range angular distribution is modified by multiplying the usual Butler expression by

$$G(K^2) = \frac{\beta^2}{\beta^2 + (1/2\ \vec{Kd} - \vec{Kp})^2} \qquad (63)$$

with Kd and Kp taking on their asymptotic values. For the present case this factor varies from 94% at 0° to 56% at 180°.

Finite range effects on the p-states, illustrated in Fig. 17, are not as large, in fact they lead to a cross section slightly larger than the zero-range cross section. This result again follows from the change in sign of the 2p functions in the interior -- the negative contribution to the amplitude is diminished by the finite-range averaging.

Non-local Effects

Another effect which dampens the contribution from the interior is due to the non-locality of the potential. As you know from the work of Brueckner and co-workers , the self-consistent Hartree-Fock potential is momentum dependent. This effect manifests itself in the local optical model treatment of scattering by making the potential energy dependent.

However, there is an additional effect, which is unimportant for scattering, which causes the relative wave functions to be reduced in the interior. Loosely speaking, this comes about because the momentum dependence manifests itself in coordinate space by introducing surface corrections to the potential. These give rise to increased reflections and diminish the wave function in the interior. The asymptotic behavior is unaffected. Perey,[14] by comparing the total wave functions from the local and non-local potentials for nucleons, has suggested that the relationship between them is

$$\psi_{NL}(r) = \frac{C}{[1 + (\beta^2/4)\, U_L(r)]^{1/2}}\, \psi_L \qquad (64)$$

where $\beta \approx .85$ fm is the range of the non-locality and

$$U_L(r) = \frac{\hbar^2}{2M}\,[V(r) + i\,W(r)] \ .$$

(More recently, Ferey and Saxon have derived this result.) Since for the scattering problem ψ_L and ψ_{NL} are equal asymptotically, $C = 1$. For the bound state wave function we must use the normalization condition

$$\int |U_{lsj}(r)|^2\, dr = 1 \qquad (65)$$

which gives

$$C > 1 \ .$$

Thus all wave functions are smaller on the interior than the local corresponding wave functions.

This form of correction can be trivially applied to the zero-range approximation by defining a new form factor as a product of the old form factor times the three non-local corrections.

Perey has applied these ideas to the $^{40}Ca(d, p)$ and $^{90}Zr(d, p)$ stripping reactions. He finds that the contributions from the interior are indeed diminished but the magnitude is relatively unchanged from the calculations without a cutoff, due to the non-local enhancement of the bound state tail. These calculations will be published shortly. Here we demonstrate the effect by dampening the interior by 50% with a smooth transition to no dampening with a function of the Saxon shape, as illustrated in Fig. 18. The cross section is indeed diminished but the shape is unchanged relative to the no cutoff calculations. The calculation with a cutoff of 4 fms is shown for comparison.

Spin Effects

Thus far we have neglected the spin effects. These can be included by the addition of spin-dependent terms in the optical model wave functions and the bound state wave function. For the neutron and proton the interaction is of the vector spin-orbit type

$$V_{so}(r) \sim \lambda \, (S \cdot L) \frac{dV(r)}{dr} . \tag{66}$$

For spin-one particles Satchler has suggested the vector spin-orbit force or tensor forces. Calculations to date have only made use of the vector spin-orbit form.

The optical model wave functions are now matrices in spin-space, e. g. ,

$$\chi^{(+)} \rightarrow \chi^{(+)\,S}_{m',\,m} \tag{67}$$

where the subscripts m' allow for a spin-flip by the spin dependent force.

The partial waves are now J dependent as well as L dependent

$$\chi_L(r) \rightarrow \chi_{J,\,L} \tag{68}$$

with

$$\vec{J} = \vec{L} + \vec{S} \ .$$

The angular momentum albegra is somewhat more complicated and will not be discussed here, a full discussion can be found in reference 3.

Spin effects can be divided into two types, effects on the magnitude, and changes in the shape of the angular distributions. In this section we consider the effect on magnitude. The change in magnitude arises mainly from the change in shape of the bound state wave function. This occurs because the Saxon well which binds the neutron is of the form

$$V(r) = V_o(r) + a(L)\,\frac{\lambda}{r}\,\frac{d}{dr}\,V_o(r) \tag{69}$$

where

$$a(L) = -L \quad \text{if } J = L + 1/2$$
$$= (L + 1), \quad J = L - 1/2 \ .$$

Thus for neutrons captured into the J = L + 1/2 orbit, the spin-orbit interaction is attractive and surface peaked. The bound state wave function is expanded. For the opposite spin state, J = L - 1/2, the wave function is contracted. If the spin-orbit well is 8 MeV (pion units) deep the effect

is to increase the calculated cross section by some 25% for the ground state transition (J = 7/2, L = 3). If an 8 MeV spin orbit interaction is included in the proton channel, the cross section is further increased -- to some 30% greater than the calculation without spin-orbit. Adding a 5 MeV spin orbit to the deuteron well compensates for the proton spin-orbit interaction, bringing the cross section to only 21% greater than the spinless case. These values of the spin-orbit strengths assigned to the proton and neutron well are close to those found to fit experimental data. The deuteron spin-orbit strength is not as well established. In general it is not needed to fit deuteron elastic data. Thus inclusion of spin orbit coupling changes our estimate of the strength S by some 20% (smaller).

A similar study on the excited p states showed the magnitude difference to be almost negligible, some 5% greater for the $P_{3/2}$ state and 5% smaller for the $P_{1/2}$ state.

If now finite range and spin orbit coupling are included, they tend to compensate, as can be seen from the table of spectroscopic amplitudes in the rows labelled ZS.

To summarize the results that have been discussed thus far, we cay say that the zero-range approximation without corrections has given a fairly good description of the $^{40}Ca(d, p)^{41}Ca$ stripping reaction. The spectroscopic amplitudes found from this work are within 20% of what is expected on the shell model. This agreement might be considered fortuitous inasmuch as we have included contributions from the interior. For the ground state transition we have seen that relaxing the zero-range

approximation by allowing the n-p force to have a finite range does not change the shape of the theoretical cross section but does decrease its magnitude, thereby leading to an increased spectroscopic amplitude S. Spin-orbit coupling, especially in the bound state function, has the opposite effect on the ground state transition, yielding a 20% increase in the absolute magnitude. A combination of these two corrections gives magnitudes comparable to those found in the zero-range approximation without a cutoff. On the other hand, both the finite-range correction and the neutron spin-orbit correction are negligible for the excited states. A rough summary of these effects is given in Table III.

Another source of uncertainty are the optical parameters. As we have seen, equivalent potentials which give the same elastic scattering give different results for stripping, especially in magnitude. Additionally, potentials which do not fit the elastic data, correctly predict the shape of the angular distribution around the main peak, but again with incorrect magnitude. Further, the shape of the angular distributions at large angles is only roughly reproduced and is critically dependent on the optical parameters chosen. This point will be discussed again.

For heavier nuclei the uncertainty in which set of optical parameters to use has been somewhat alleviated by the systematic parameter surveys of Perey[8] for protons and by Perey and Perey[10] for deuterons. A word of caution is in order here, these parameters should not be extrapolated, either in energy or in A, beyond the bounds considered by these papers. Interpolation, on the other hand, is reasonably safe.

Finally it should be pointed out that relative magnitudes of peak cross sections are less dependent on these uncertainties, except perhaps for the spin-orbit dependence, and should be more reliable than absolute values.

J Dependence of the Angular Distributions

These measurements show quite different angular distributions at large angles for stripping with the same ℓ transfer but with different J-values. In Fig. 15 this is illustrated for the 12 MeV measurements. The data (black circles) for the $P_{1/2}$ angular distribution shows a deep minimum at 100°, while this minimum does not appear in the $P_{3/2}$ differential cross sections. (The filling in the minimum after the main stripping peak is a Q effect.) Schiffer and Lee have found that this systematic difference persists for other (d, p) reactions in this mass region and have used it to identify the J-value of the neutron orbital.

Qualitatively, the origin of this difference can be explained, if the spin-orbit distortions are treated as perturbations. Johnson[15] has shown that then the cross section can be written as the sum of two terms,

$$\frac{d\sigma}{d\Omega} = A(\theta) + (-)^{J-\ell-1/2} B(\theta) \qquad (70)$$

with $A(\theta)$ arising from the central well distortions and $B(\theta)$ proportional to the spin-orbit strengths of the optical wells. Thus we may have constructive or destructive interference at some large angle depending on the J of the captured neutron.

Distorted wave calculations have been made to see if the theory can explain this effect. It was found that spin-orbit interaction in the bound state well produced no shape changes, but that spin-orbit distortions in either channel do indeed produce such changes (shown in Fig. 15). Here the theory gives a shallow minimum for the $P_{1/2}$ case but also predicts a minimum at large angles for the $P_{3/2}$ groups which is not observed experimentally. Additionally, examination of other data indicates that this effect is not reliably reproduced, either as a function of energy or target mass, if best fit elastic parameters are used. However, Rost has been able to find this effect in many cases by allowing only proton spin-orbit distortion, but the other proton parameters are allowed to be relaxed from their best fit values.

In short, the distorted wave approximation is capable of explaining such phenomena, but is as yet incapable of giving a detailed account. Indeed, as can be seen from Fig. 8, the theory does not well reproduce the 2nd peak in the ground state angular distribution which is much larger than the J-dependent effects. Until this can be explained, it is premature to ask more detailed questions about small effects.

Effective Binding Energy

The calculations discussed thus far make use of a bound state function, $u_{n\ell}(r)$, defined by the overlap of the target and residual nuclei. Here n is the principal quantum number and again ℓ the orbital angular momentum of the captured neutron. As has been mentioned, this function is taken as an eigensolution of the Schrödinger equation with a well of

the Woods-Saxon shape. We have no a priori knowledge of the shape or depth of this well. We can postulate that the wave function from the true "single particle" well might have a different shape than we are using.

For the states of a single nucleon added to an inert core, our simple prescription might be reasonable, this well could then be interpreted as the shell model well. If, however, the core is polarized by the additional nucleon, or if there are several particles outside a closed shell, deviations from the shell model might be expected -- in the first case through the re-arrangement of the core nucleons, in the second case through the residual interactions of the extra-core nucleons. A direct manifestation of this effect is a shift in binding energy away from that given by the shell-model for a particular orbital.

The question arises as to how to best represent this function. We know that asymptotically the wave function behaves like

$$\frac{e^{-Kr}}{r} \tag{71}$$

with the wave number K proportional to the square of the separation energy.

$$\epsilon_s = \epsilon_d + Q . \tag{72}$$

One school of thought then argues that the wave function should be an eigensolution with this eigenvalue.

Alternatively, the true wave function can be expanded in a complete set of shell model wave functions, including the continuum of this set.

It is then argued that one should use the shell model orbital with the same quantum numbers as the true single particle orbital, on grounds that it is the largest component. Thus we would solve for a function with some effective energy, $\epsilon_{eff} \neq \epsilon_s$. In the spirit of the shell model this would imply describing all the single particle functions of a given nucleus as eigensolutions of a well with constant depth.

The point is important because the magnitude of the wave function in the region of strong overlap with the distorted waves directly affects the measure of the spectroscopic amplitude S. For $\epsilon_{eff} < \epsilon_s$, the wave function expands. For $\epsilon_s < \epsilon_{eff}$ the wave function contracts.

Most distorted wave stripping calculations have used the separation energy. The evidence for the other prescription is mixed.

The clearest evidence for this concept was found in the (p, d) reactions on the isotopes of Fe.[16] This reaction excites the T ± 1/2 states of the same shell model configuration which differ by several MeV. To obtain agreement with theoretical spectroscopic factors, it was necessary to use the same binding energy for both transitions.

A shape difference was recently pointed out by Rost[17]. Two states in ^{55}Fe are excited by the (p, d) reaction on ^{56}Fe. Both are $\ell = 3$, but with $J = 7/2$ and $5/2$. They differ in excitation by only .4 MeV. To obtain agreement with the shapes of the angular distributions, Rost adjusted the depth of the central well binding the $f_{5/2}$ particle until it agreed in depth with the central well binding the $f_{7/2}$ particle. The agreement is quite good as is seen in Fig. 19.

On the other hand Satchler has found contrary evidence in an analysis of ^{43}Ca(d, t) reactions. He obtains good agreement with theoretical predictions by using the separation energy. On the other hand, if a constant well is used for all transitions, he finds the ground state spectroscopic amplitude a factor of two too large.

For the present case ^{40}Ca(d, p)^{41}Ca, the two $P_{3/2}$ states are candidates for such a study. Here for the state at 2.5 MeV, the separation energy for the 2 MeV state was used, (6.42 MeV), resulting in a 15% decrease in cross sections which, incidentally, makes the sum of the $S_{3/2}$ strengths exceed unity.

This conflicting evidence indicates that no simple prescription can be given, each nucleus must be examined separately. More work, both theoretical and experimental, is needed.

Other Single Nucleon Transfer Reactions

We have discussed most of the current ideas on the theory of stripping reactions and have seen that the theory has given reasonable results, although some uncertainties and discrepancies in fit still remain. The disagreement of the theory with the experimental second maximum of the ground state group is especially significant and indicates that we are neglecting an important part of the amplitude.

The situation for heavy nuclei is somewhat better as Fig. 20 shows, for the (d, p) reactions on cadmium-114. These data were taken by Silva et al.[19] at Oak Ridge and were analyzed using the parameters of the Perey's[11] which give a good account of the deuteron elastic scattering. No parameters were juggled and the curves

shown did not use any cutoffs of the radial integrals. The spectroscopic amplitudes are in fair agreement with pairing theory calculations.

This is not always the case, for example Miller et al.[20] were unable to find a set of deuteron parameters which could simultaneously explain the elastic scattering of deuterons and the stripping angular distributions for ^{206}Pb.

The situation for light nuclei is as yet unclear, no systematic analyses of elastic scattering and stripping have been completed although one is in progress at Oak Ridge. Some preliminary results for the ^{16}O(n, d)^{15}N ground state transition, (ℓ = 1), are available. The measurements were taken at Zagreb with 14 MeV neutrons and the analyses done at Oak Ridge. Again this is a favorable case for testing the ability of the DWBA to give absolute spectroscopic factors. On the shell model ^{16}O is doubly magic and the expected spectroscopic factor is two.

Data is available for 14 MeV neutron scattering from ^{16}O and parameters similar to these found by Perey[8] give a good account of the angular distribution as seen in Fig. 21.

For the exit channel parameters which fit the elastic scattering of 8 MeV deuterons from ^{16}O were used, Fig. 22, since there isn't any data for the scattering of 4 MeV deuterons from ^{15}N. Several variations of the deuteron optical parameters were also tried.

The agreement with the pickup data is very good provided one allows spin-orbit coupling in the well which binds the proton and uses the finite range form of the theory. On the other hand, to find agreement with the data using the zero-range approximation we must invoke a radial cutoff, even then S is reduced to 1.63.

Figures 23 and 24 show the results of these calculations with the Zagreb data. The first of these uses a deuteron potential with the imaginary potential surface peaked, the second uses an imaginary potential of the Woods-Saxon shape. Although there are differences either one gives a reasonable prediction to the shape and the correct magnitude with S = 2. Still another calculation was tried varying the deuteron parameters slightly from those shown in Fig. 22 . In particular, a was changed from 0.9 fms to 0.8 fms, r'_o from 1.85 fms to 1.8, and V increased by 10 MeV. The predicted shape is quite good but the magnitude changed by 50%, yielding S = 3, illustrating again that incorrect conclusions can be drawn if the wrong optical parameters are used.

Single nucleon stripping and pickup reactions involving other ions, e.g., (^{3}He, d) or (d, ^{3}He), are treated in much the same way. Aside from the uncertainties of treating the relative wave functions in the optical model approximation and what to take as the interaction, there is an additional complication, namely the unknown overlap of the internal wave functions of the particles. To date, this knowledge is unavailable and the distorted wave theory is left with an unknown normalization. Until more details of the configurations of these ions are known, this normalization must be extracted from experiment, using target nuclei where the spectroscopic factors are reasonably certain.

Some work has been done on the ^{40}Ca(d, ^{3}He)^{39}K and ^{40}Ca(^{3}He, d) reactions, and the theory works quite well. The normalizations extracted from these calculations agree to within 30% and it appears that we will be able to use these reactions to extract absolute spectroscopic factors. Much work remains to be done.

Inelastic Scattering

This subject has been covered in some detail in the literature,[21] and in the proceedings of various summer schools.[1] In these notes only the main ideas will be reviewed and some recent applications to light nuclei discussed.

From the previous considerations on stripping we have seen that stripping and pickup reactions give information about single particle (hole) states of nuclei. The approximation that is taken and which has proven fairly good is that only the interaction between the stripped particle and the outgoing particle need be considered.

Inelastic scattering is somewhat different. In this case many nucleons in the target can be involved. Neglecting spin-flip, the interaction between target and projectile can be expanded in multipoles of angular momentum transfer L

$$V(\vec{r},\ \epsilon) = \sum_{L,\,M} (i^{L})\ V_{L}(r,\ \epsilon)\ Y_{L}^{*m}(r) \tag{73}$$

and the nuclear matrix element becomes

$$\langle \varphi_{A^*} |\ V_{L}\ (r,\ \epsilon)\ |\ \varphi_{A} \rangle \tag{74}$$

where target A has been excited to A*. From this point two approaches have been considered. In the first it is assumed that there is detailed knowledge of the nuclear wave functions φ_A, and φ_{A^*}, and the interaction of the incoming projectile with the constituent nucleons of the target, i. e.,

$$V_{L}\ (r,\ \epsilon) \equiv \sum_{i} V_{L}\ (r - r_{i}) \tag{75}$$

where i labels the coordinate of the ith nucleon, and the sum extends over all the active nucleons.

This method has been discussed in detail by Levinson and Bannerjee[22] for the $^{12}C(p, p')^{12*}C$ reaction and more recently by Funsten and Rost[23] for inelastic scattering of protons from nuclei in the $f_{7/2}$ shell. In the first case, only nucleons in the p shell were considered, in the second, only f particles were included. Agreement with data is found only if the interaction strength is taken some two to three times that needed to explain nucleon-nucleon scattering at low energies. Additionally, Levinson and Bannerjee were forced to depart from parameters which fitted elastic proton scattering from carbon. On the other hand, Funsten and Rost used parameters consistent with those found by Perey.

The discrepancies in strength are attributable to neglecting the many other possible configurations which can participate in the reaction. Calculations which use better nuclear wave functions are underway at Oak Ridge.

Another approach which avoids the question of which nucleons are participating is to be described by the collective model,[24] wherein the surface is deformed (or deformable) and is characterized by the radius parameter

$$R = R_0 \left(1 + \sum \alpha_{kq} Y_k^q \left| \theta' \varphi' \right.\right)$$

$$= R_0 + \delta R \ . \qquad (76)$$

Here the α_{kq} are the collective coordinates and θ' and φ' are polar angles relative to body fixed axes.

It is reasonable to assume that the interaction between the projectile and the target is also non-spherical and depends on the distance from the surface R as defined above.

We then take the potential V(r - R) and expand it in a Taylor's series

$$V(r - R) = V(r - R_0) - \delta R \frac{d}{dr} V(r - R)\Big|_{R=R_0} + \frac{1}{2} \alpha R^2 \Big|_{R=R_0} + \ldots \qquad (77)$$

In the perturbation limit the first term gives elastic scattering, the second term taken once leads to single excitation of the nucleus. The second term taken twice gives double excitation but is not computable in distorted wave approximation, since it refers to a two-step process. The third term also yields double excitation, and is treatable in first approximation, but it is inconsistent to treat the direct term without taking into account two-step processes.

The reactions which can be treated in the usual DWBA manner are, therefore, single excitations and the interaction is proportional to

$$\langle \varphi_{A*} \Big| \delta R \frac{dV}{dr} \Big| \varphi_A \rangle \ . \qquad (78)$$

For collective rotations, the α_{kq} can be written as

$$\alpha_{20} = \beta \cos \gamma$$

$$\alpha_{2\pm1} = 0$$

$$\alpha_{2\pm2} = \beta \sin \gamma$$

with β the usual deformation parameter, and γ the assymetry. For axially

symmetric nuclei $\gamma = 0$. Then the interaction is, for a quadrupole deformation,

$$V^{(1)} = - R_0 \beta \frac{dV}{dr} (r - R_0) Y_2 \tag{79}$$

with respect to body fixed axes. Thus one number is extracted from comparison of theory with experiment, the deformation parameter β.

For collective vibrations, the a_{kq} are interpreted as a linear superposition of boson destruction and creation operators

$$a_{kq} = \sqrt{\frac{\hbar w_k}{2C_k}} \left[b_{kq} + (-)^q b^*_{k\,-\,q} \right]. \tag{80}$$

Here hW_k is the phonon energy and C_k is the restoring parameter. The interaction then is

$$V^{(1)}_{\ell m} = i^{\ell} R_0 \frac{dV(r - R_0)}{dr} a^*_{\ell m} \tag{81}$$

and the nuclear matrix element yields

$$\langle \varphi_{A^*} | a^*_{\ell m} | \varphi_A \rangle = \frac{\sqrt{\hbar W_\ell}}{2C_\ell} \tag{82}$$

which can be interpreted as an effective (rms) deformation

$$\beta = \sqrt{2\ell + 1} \sqrt{\frac{\hbar W_\ell}{2C_\ell}} \,. \tag{83}$$

It is impossible to distinguish between rotational and vibrational excitation in first order.

A literal interpretation of these formulae suggests that the parameters of the form factor are the same as the optical potential which explains elastic scattering. All calculations to data, in which DWBA is expected to apply, have agreed with this supposition. Thus once the elastic scattering has been fitted, the inelastic scattering angular

distribution is predicted and agrees quite well with measurements. This theory has been used with fair success to explain collective excitations in medium light nuclei.

Recently, the theory has been applied to the excitation of ^{12}C by 126 MeV ^{12}C ions and by 168 MeV oxygen ions. Figures 25 and 26 show the optical model fits to the relevant elastic data, and Figs. 27 and 28 the DWBA predictions for the excitation of the 2+ (4.43 MeV) state in ^{12}C. The deformation β listed in Fig. 27 should be replaced by 0.8.

Analyses of the excitation of this state by α-particles yields $\beta = 0.5$. So there is major disagreement between the deformations extracted from different experiments.

Our previous discussion has shown that the nuclear matrix element has amplitude

$$A_{lSJ,m} = \frac{\beta R_0 V}{a} .$$

Blair has suggested that since the interaction radius R_0 is not uniquely determined, these measurements do not give β but the combination βR_0. Applying this we find for the excitation of the 2+ state by α-particles $\beta R_0 = 2$ fms, while the excitation by ^{12}C and by oxygen give $\beta R_0 = 1.8$ fms, and 1.73 fms, respectively.

In the oxygen + carbon experiment cited above, the 3^- state in oxygen is also excited. Again the DWBA theory gives a reasonable prediction of the cross section, as shown in Fig. 29. It appears that inelastic scattering from light nuclei at sufficiently high projectile energies can be easily interpreted and gives consistent spectroscopic information.

Acknowledgments

The author gratefully acknowledges his colleagues, G. R. Satchler and R. M. Drisko, for helpful conversations and their advice.

REFERENCES

1. N. Austern in Fast Neutron Physics, II, ed. by J. B. Marion and J. L. Fowler (Interscience Publishers, Inc., New York, 1963); selected topics in Nuclear Theory, ed. by F. Janouch (I. A. E. A., Vienna, 1963).
2. E. Gerjuoy, Annals of Physics 5, (1958).
3. G. R. Satchler, to be published in Nuclear Physics.
   R. H. Bassel, R. M. Drisko, and G. R. Satchler, "The Distorted Wave Theory and the Code Sally," ORNL Report 3240.
4. N. Austern, R. M. Drisko, E. C. Halbert, and G. R. Satchler, Phys. Rev. 133, B3 (1964).
5. M. H. McFarlane and J. B. French, Rev. Mod. Phys. 32, (1960).
6. J. B. French in Nuclear Spectroscopy, B, ed. by F. Ajzenberg-Selove (Academic Press, New York, 1960).
7. L. L. Lee, J. P. Schiffer, B. Zeidman, and G. R. Satchler, R. M. Drisko, and R. H. Bassel, to be published in Phys. Rev.
8. F. G. Perey, Phys. Rev. 131, 745 (1963).
9. G. R. Satchler, to be published.
10. E. C. Halbert, Nucl. Phys. 50, 353 (1964); C. M. Perey and F. G. Perey, Phys. Rev. 132, 755 (1963).
11. R. M. Drisko, G. R. Satchler, and R. H. Bassel, Physics Letters 5, 347 (1963).
12. N. Austern, Ann. Phys. 15, 299 (1961).
13. P. E. Hodson, Direct Interactions and Nuclear Reaction Mechanisms, ed. by E. Clementel and C. Villi (Gordon and Breach, New York, 1963).
14. F. G. Perey, Direct Interactions and Nuclear Reaction Mechanisms.

15. R. C. Johnson, private communication.

16. E. Rost, B. F. Bayman, and R. Sherr, Bull. Am. Phys. Soc. 9, No. 4, 1964.

17. R. Sherr, E. Rost, and M. E. Rickey, to be published in Phys. Rev. Letters.

18. G. R. Satchler, et al., to be published.

19. R. J. Silva and G. E. Gordon, to be published in Phys. Rev.

20. D. W. Miller, H. E. Wegner, and W. S. Hall, Phys. Rev. 125, 2054 (1962).

21. R. H. Bassel, G. R. Satchler, R. M. Drisko, and E. Rost, Phys. Rev. 128, 2693 (1962), and references therein.

22. C. Levinson and M. K. Bannerjee, Ann. Phys. 2, 471 (1957); and Ann. Phys. 3, 67 (1958).

23. H. O. Funsten, N. Roberson, and E. Rost, Phys. Rev. 134, 1B, 117 (1964).

24. A. Bohr and B. Mottelson, Kgl. Danske. Videnskab, Selskab, Matt-fys. Medd. 27, No. 16 (1953).

TABLE I

Optical Parameters for 11 MeV Deuterons on Calcium-40

Potential	V(MeV)	W(MeV)	r_o(F)	a(F)	r_w(F)	a_w(F)	W_D(MeV)	σ_R(mb)
X	32.5	0	.943	.905	1.7	.691	5.6	1353
Y	72.4	↓	.936	.943	1.5	.542	11.8	1163
Z	120.7	↓	.966	.846	1.48	.492	16.4	1133
G	176.9	↓	1.002	.769	1.47	.453	21.0	1117
F	240.0	↓	1.04	.707	1.46	.415	26.4	1104
J	307.0	↓	1.09	.651	1.47	.368	34.5	1092
K	406.0	↓	1.07	.633	1.47	.359	37.8	1095
L	460.0	↓	1.154	.573	1.49	.304	51.5	1085

TABLE II

Spectroscopic Factors

Q (MeV)		7 MeV	8 MeV	9 MeV	10 MeV	11 MeV	12 MeV	Average
6.14	Peak (mb/st)	4.2	4.4	5.15	5.37	6.55	5.65	
	S (Av. Z)[a]	.928	.866	.925	.894	.943	.876	.91 ± .03
	S (Best Z)[a]	.742	.934	.891	.831	.957	.832	.87 ± .07
	S (Best ZS)[b]	.813	.888	.901	.856	.959	.756	.86 ± .07
	S (Av. Z)[a,c]	1.54	1.52	1.70	1.68	1.99	1.63	1.67 ± .16
4.19	Peak (mb/st)	22.5	25.0	31.5	27.5	34.8	30.0	
	S (Av. Z)[a]	.695	.676	.788	.654	.795	.662	.71 ± .06
	S (Best Z)[a]	.843	.745	.830	.676	.713	.566	.73 ± .09
	S (Best ZS)[b]	.891	.732	.840	.532	.664	.536	.72 ± .12
3.67	Peak (mb/st)	10.7	11.0	12.7	13.5	16.5	18.0	
	S (Av. Z)[a]	.306	.276	.296	.299	.351	.369	.32 ± .03
	S (Best Z)[a]	.375	.301	.316	.307	.319	.320	.32 ± .02
	S (Best ZS)[b]	.394	.299	.316	.289	.294	.299	.32 ± .04
	S (Av. Z)[a,c]	.324	.292	.315	.317	.381	.411	.34 ± .04
3.67 + 4.19	S (Av. Z)[a]	1.001	.952	1.084	.953	1.146	1.031	1.03 ± .07
	S (Best Z)[a]	1.218	1.046	1.146	.983	1.032	.886	1.05 ± .10
	S (Best ZS)[b]	1.285	1.031	1.156	.921	.958	.835	1.03 ± .15
2.19	Peak (mb/st)	12.5	18.0	20.5	(21.9)	(23.5)	(24.0)	
	S (Av. Z)[a]	.572	.721	.760	(.77)	(.81)	(.78)	.68 ± .08
	S (Best Z)[a]	.691	.784	.820	(.8)	(.7)	(.7)	.77 ± .05
	S (Best ZS)[b]	.732	.779	.858	(.78)	(.72)	(.67)	.78 ± .04

a. Zero-range approximation without spin-orbit coupling

b. Finite-range, with spin-orbit coupling

c. Radial cut-off at 4.1F

TABLE III

Variations of Peak Cross Sections for a Deuteron Energy of about 11 MeV

Effect	$1f_{7/2}$ Q = 6.14 MeV	$2p_{3/2}$ Q ≈ 4 MeV	$2p_{1/2}$ Q = 2.19 MeV
Finite Range	- 15%	+ 1%	+ 3%
Cut-off, 4F	- 45%	- 6%	- 6%
$B_{eff} = S \mp 0.5$ MeV	± 6%	± 15%	± 15%
Neutron spin-orbit, 8 MeV	+ 25%	+ 4%	- 5%
Proton spin-orbit, 8 MeV	+ 5%	+ 3%	+ 1%
Deuteron spin-orbit, 5 MeV	- 7%	- 2%	+ 4%
Neutron radius 1.25	+ 15%	+ 10%	+ 10%

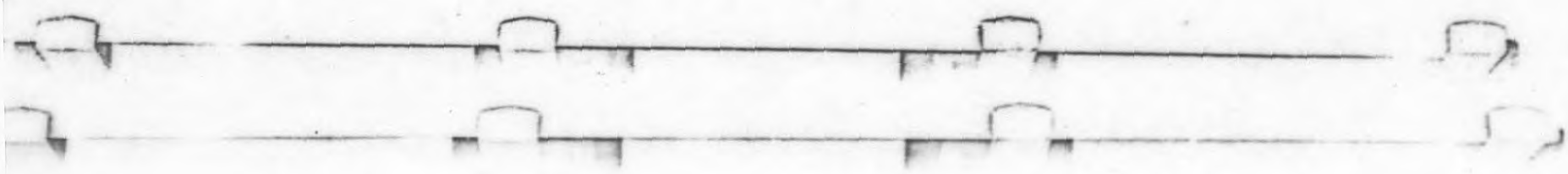

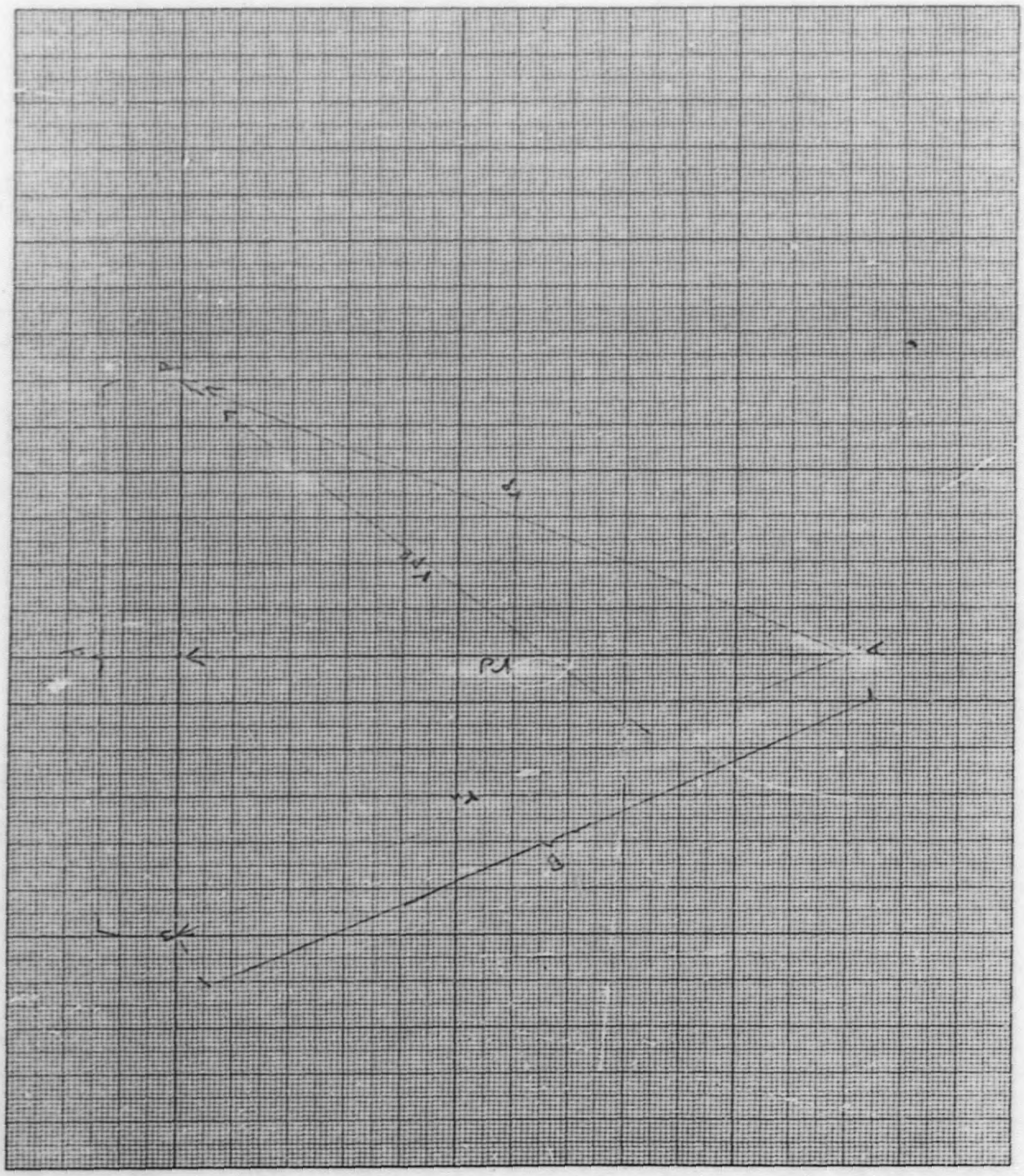

Figure 2

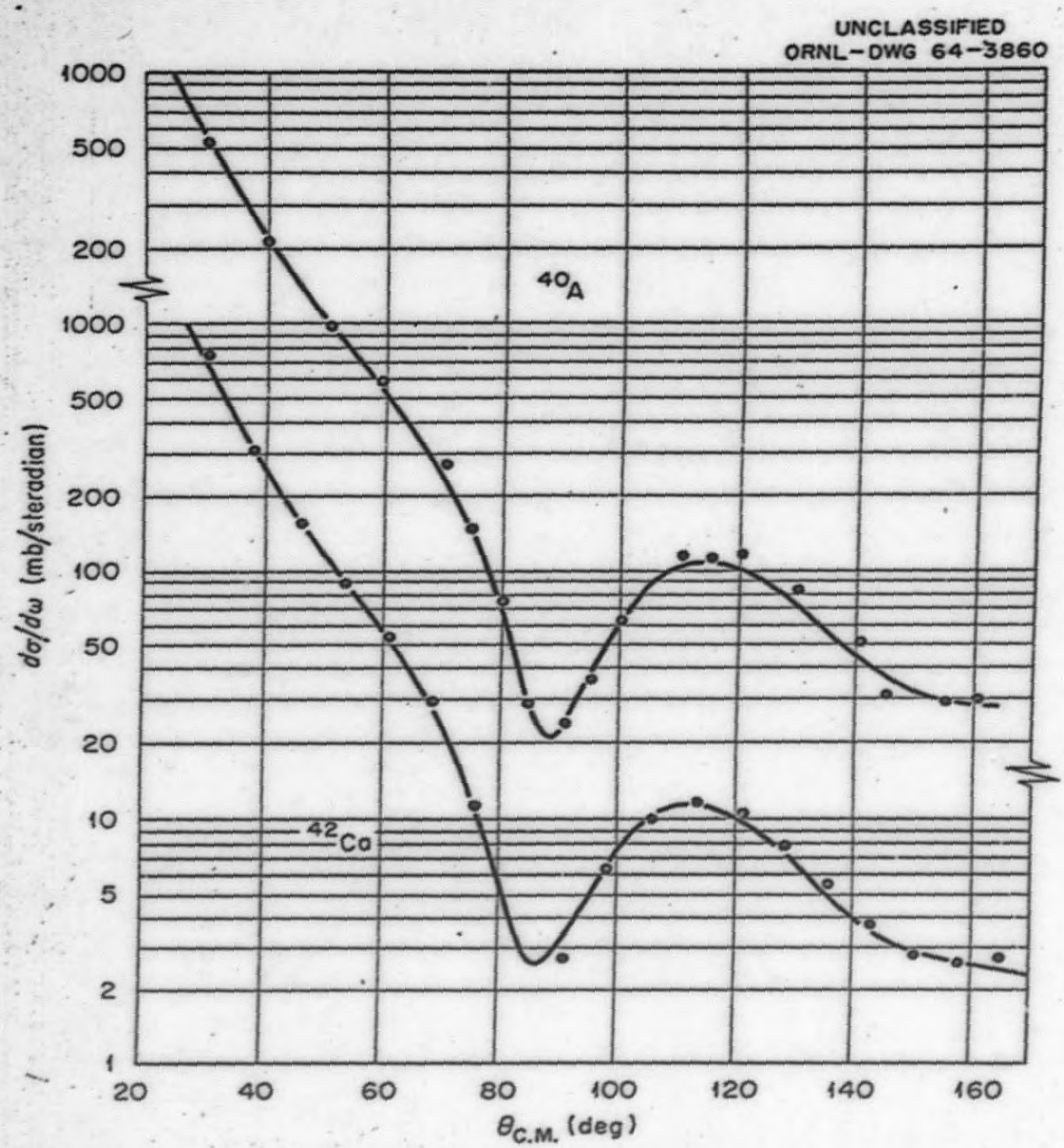
UNCLASSIFIED
ORNL-DWG 64-3860
1000
500
200
1000
500
200
100
50
20
10
5
2
1
^{40}A
^{42}Ca
dσ/dω (mb/steradian)
20
40
60
80
100
120
140
160
θC.M. (deg)

Figure 3

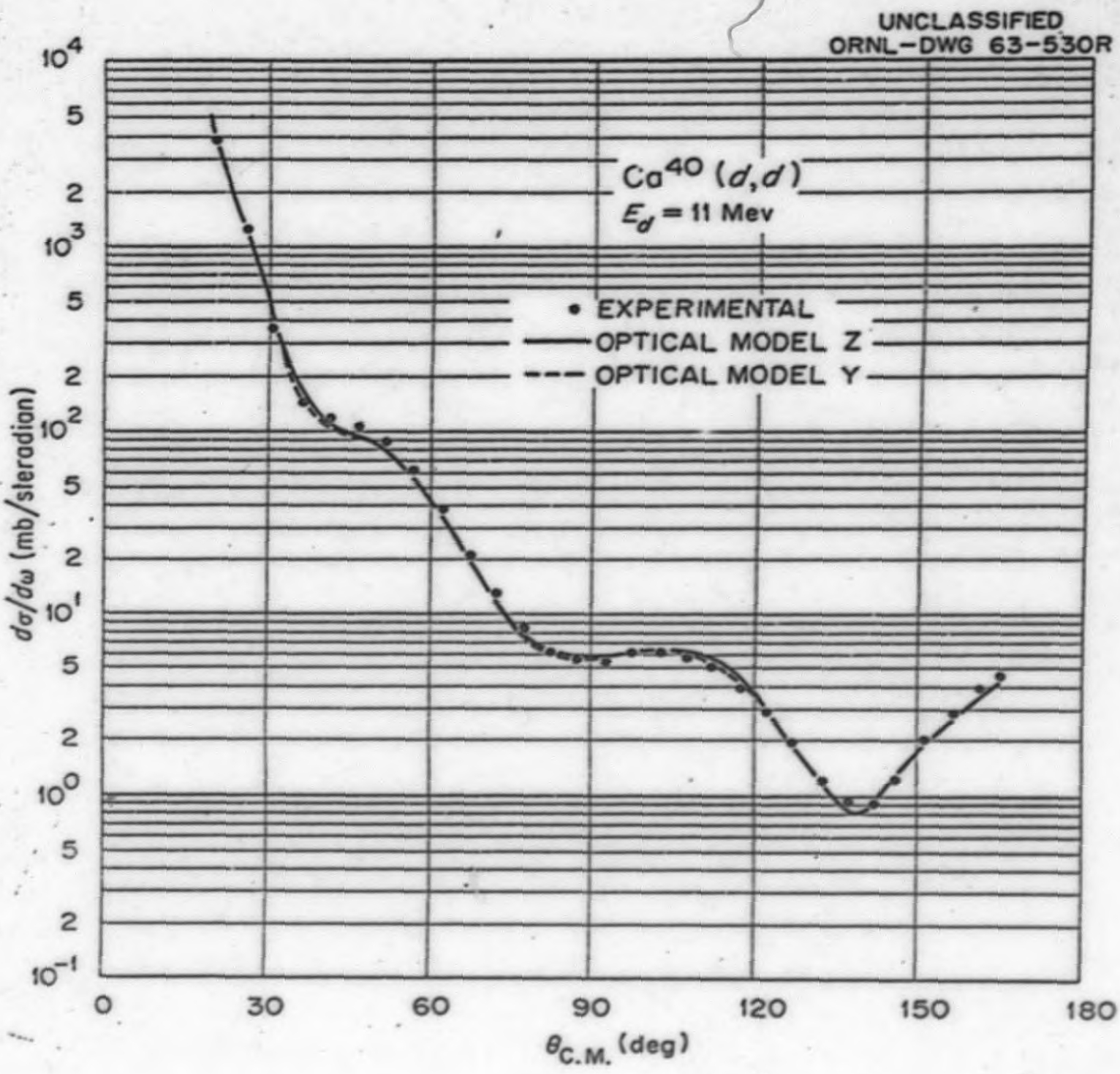
UNCLASSIFIED
ORNL-DWG 63-530R
Ca^{40} (d,d)
E_d = 11 Mev
• EXPERIMENTAL
OPTICAL MODEL Z
OPTICAL MODEL Y
dσ/dω (mb/steradian)
10^4
5
2
10^3
5
2
10^2
5
2
10^1
5
2
10^0
5
2
10^{-1}
0
30
60
90
120
150
180
$\theta_{C.M.}$ (deg)

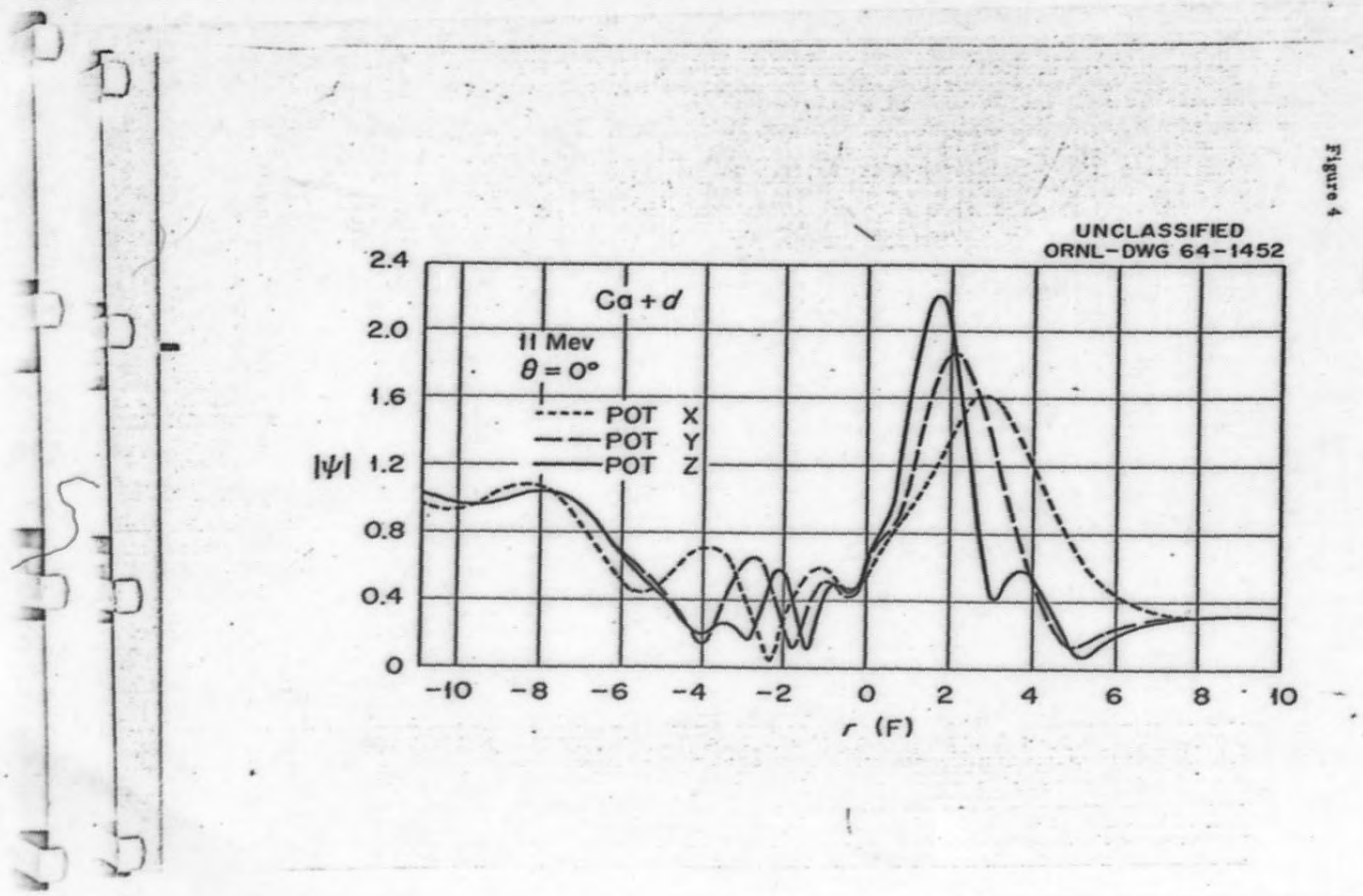
UNCLASSIFIED
ORNL-DWG 64-1452
Ca + d
11 Mev
θ = 0°
POT X
POT Y
POT Z
|ψ|
2.4
2.0
1.6
1.2
0.8
0.4
0
-10
-8
-6
-4
-2
0
2
4
6
8
10
r (F)

Figure 4

Figure 5

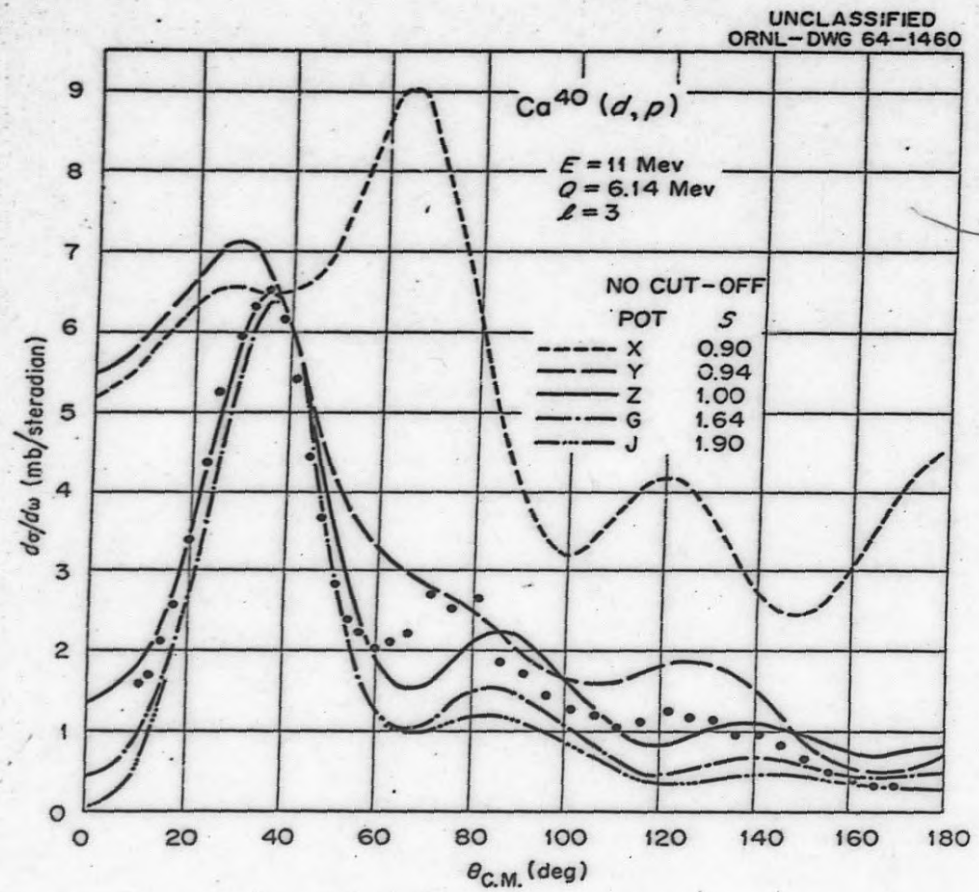
UNCLASSIFIED
ORNL-DWG 64-1460
Ca40 (d, p)
E = 11 Mev
Q = 6.14 Mev
ℓ = 3
NO CUT-OFF
POT S
X 0.90
Y 0.94
Z 1.00
G 1.64
J 1.90
dσ/dω (mb/steradian)
θC.M. (deg)
0
1
2
3
4
5
6
7
8
9
0
20
40
60
80
100
120
140
160
180

UNCLASSIFIED
ORNL-DWG 64-1459

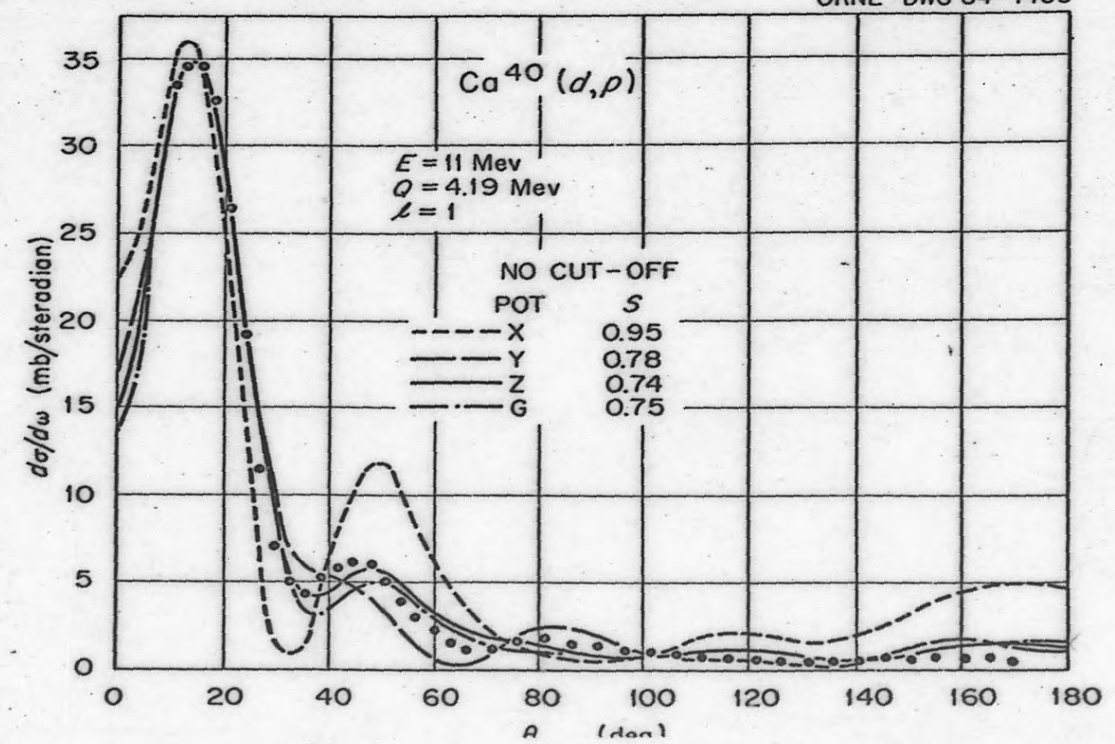

Figure 6

Figure 7

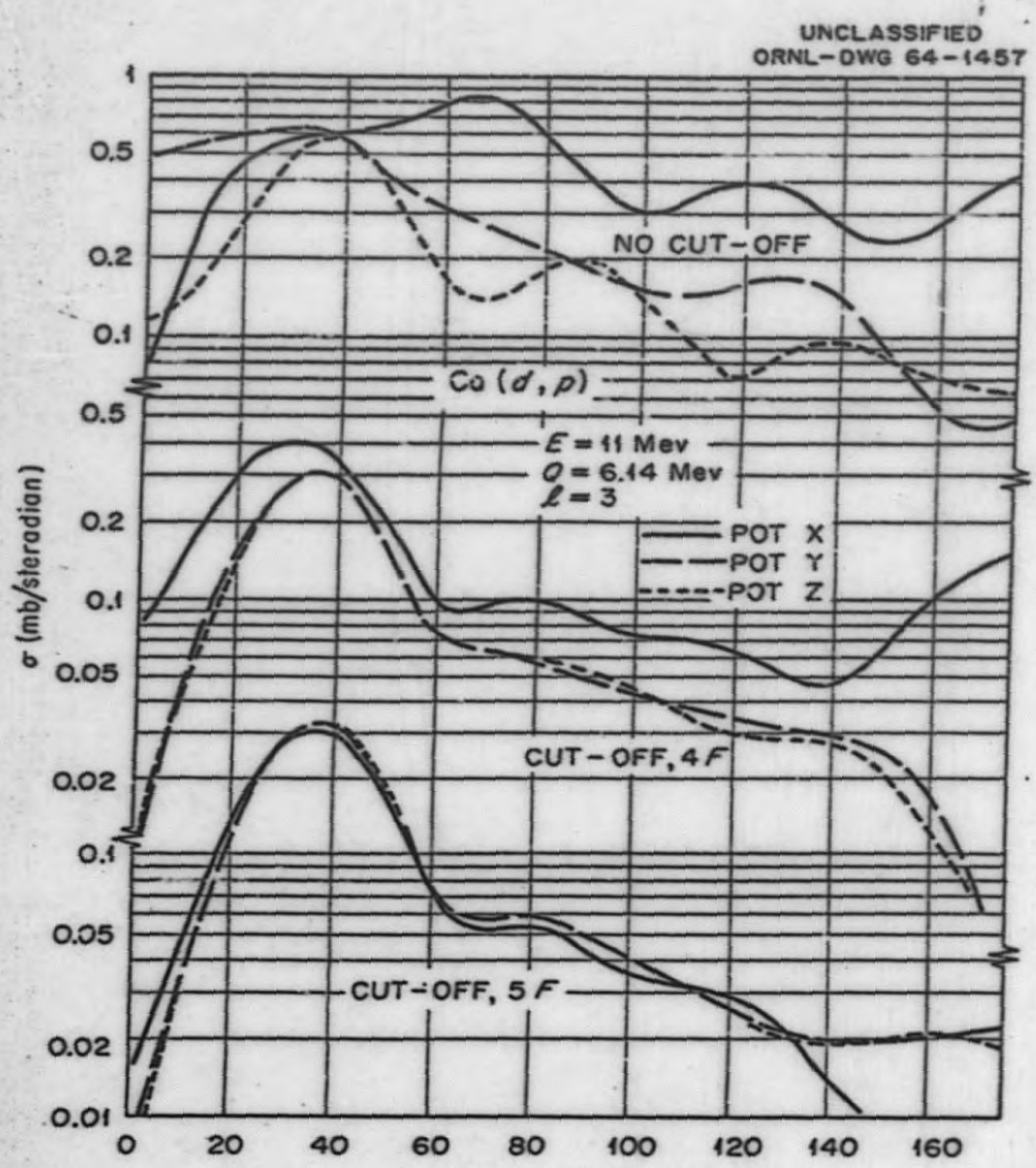
UNCLASSIFIED
ORNL-DWG 64-1457
NO CUT-OFF
Co (d, p)
E = 11 Mev
Q = 6.14 Mev
ℓ = 3
POT X
POT Y
POT Z
CUT-OFF, 4F
CUT-OFF, 5F
σ (mb/steradian)
1
0.5
0.2
0.1
0.05
0.02
0.01
0
20
40
60
80
100
120
140
160

Figure 8

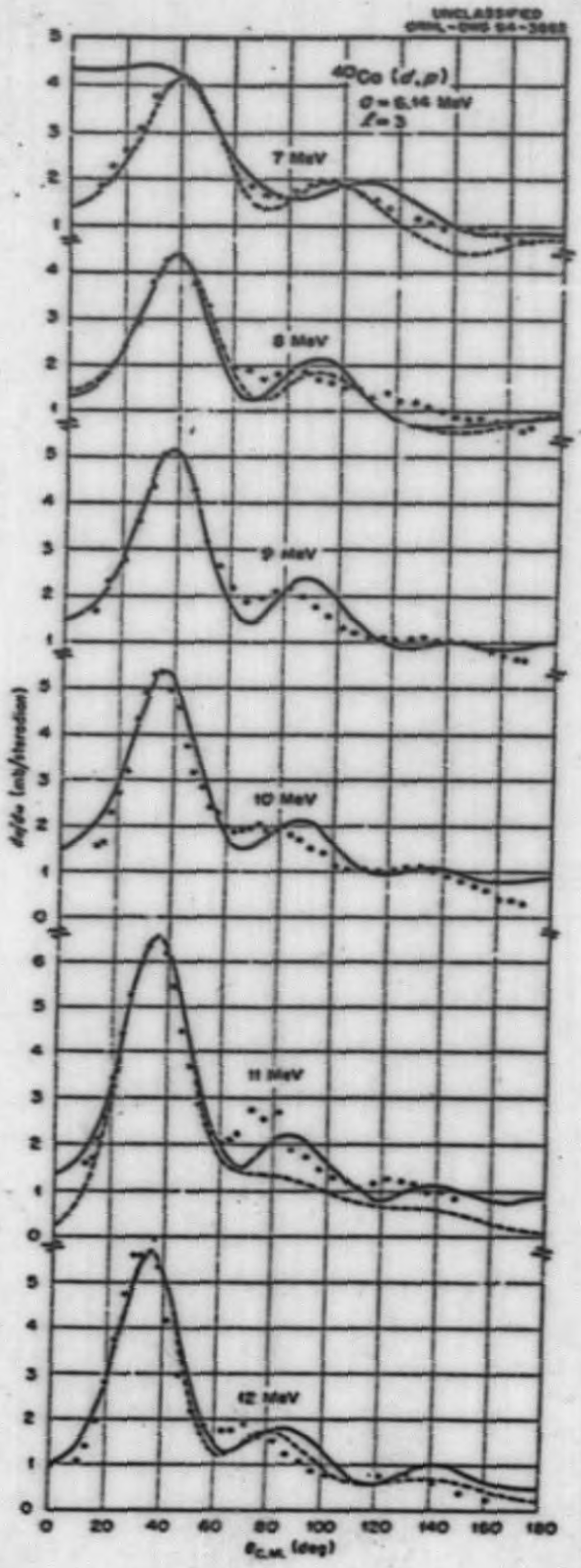
UNCLASSIFIED
ORNL-DWG 64-3865
40Ca (d,p)
Q = 6.14 MeV
l = 3
7 MeV
8 MeV
9 MeV
10 MeV
11 MeV
12 MeV
dσ/dω (mb/steradian)
0 20 40 60 80 100 120 140 160 180
θC.M. (deg)

Figure 9

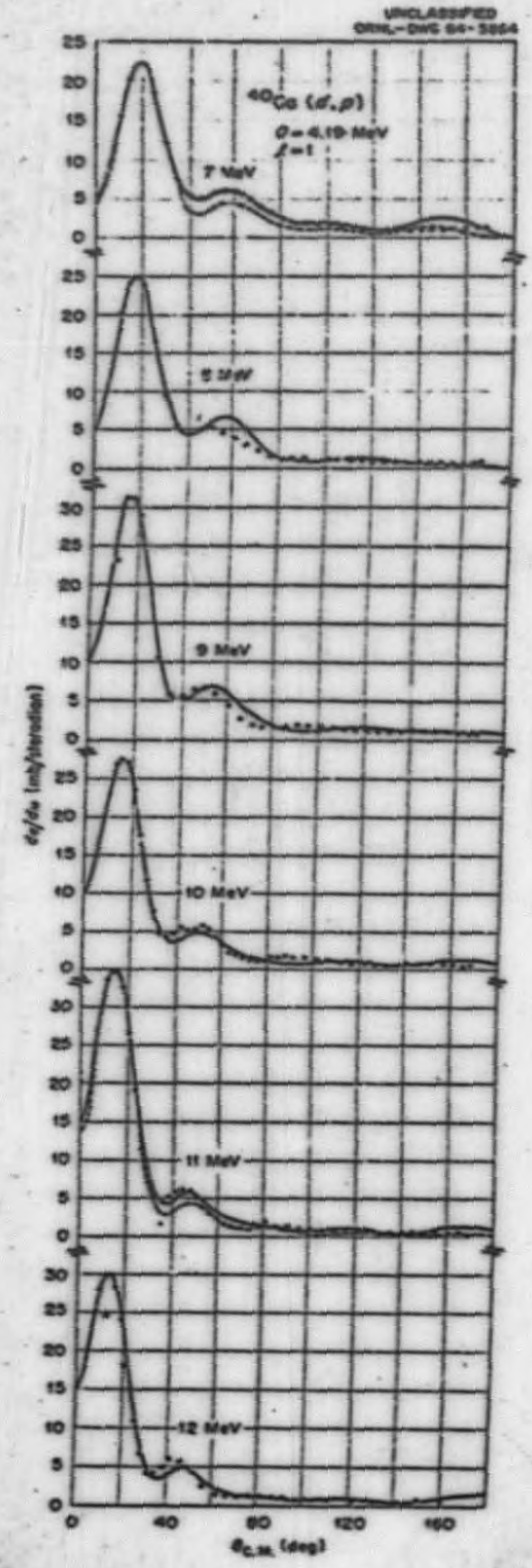
UNCLASSIFIED
ORNL-DWG 64-3864
40Ca (d, p)
Q = 4.19 MeV
ℓ = 1
7 MeV
8 MeV
9 MeV
10 MeV
11 MeV
12 MeV
dσ/dω (mb/steradian)
θc.m. (deg)

Figure 10

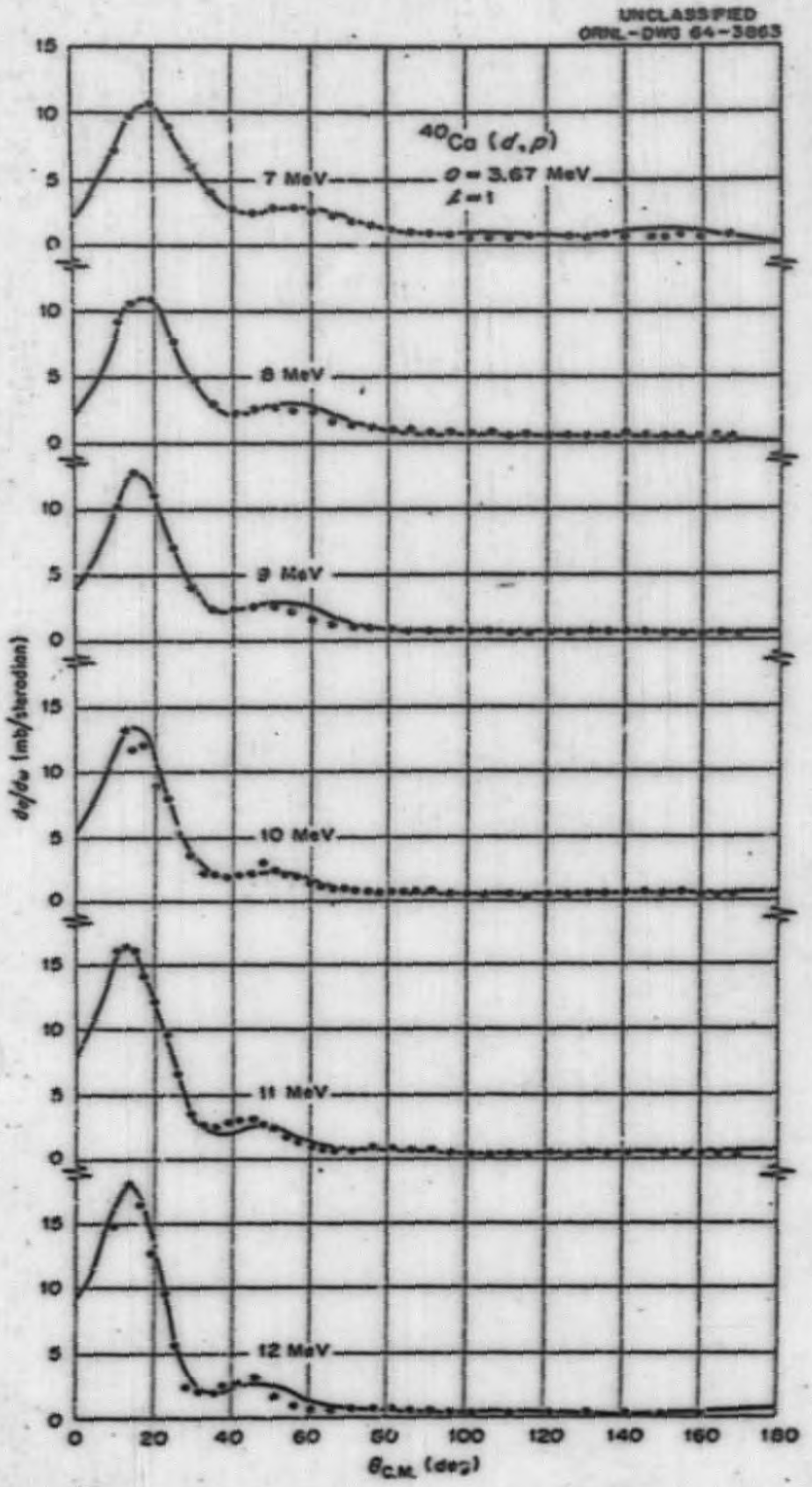
UNCLASSIFIED
ORNL-DWG 64-3863
$^{40}Ca\ (d,p)$
Q = 3.67 MeV
L = 1
7 MeV
8 MeV
9 MeV
10 MeV
11 MeV
12 MeV
dσ/dω (mb/steradian)
θC.M. (deg)

Figure 11

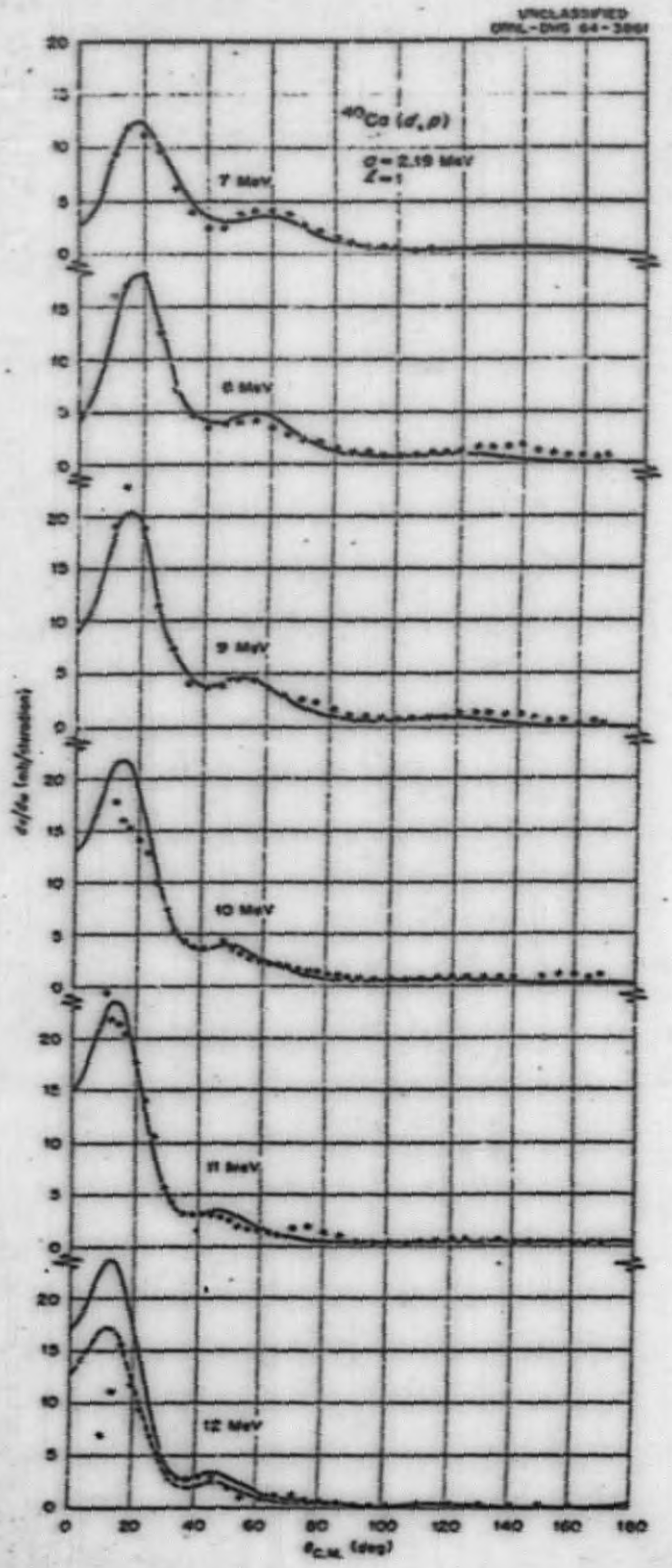
UNCLASSIFIED
ORNL-DWG 64-3861
40Ca (d,p)
Q = 2.19 MeV
L = 1
7 MeV
8 MeV
9 MeV
10 MeV
11 MeV
12 MeV
dσ/dω (mb/steradian)
θC.M. (deg)

Figure 12

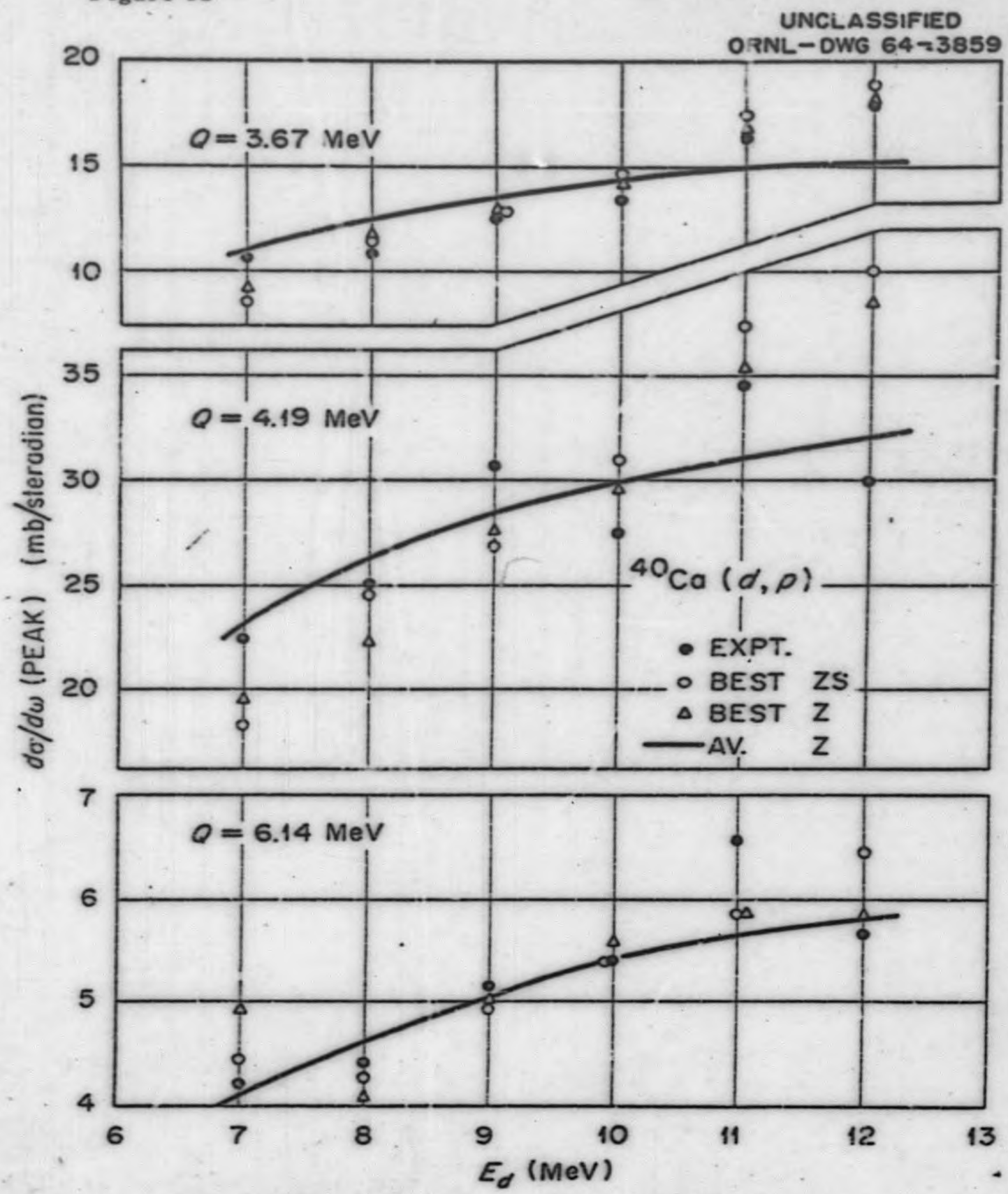
UNCLASSIFIED
ORNL-DWG 64-3859
Q = 3.67 MeV
Q = 4.19 MeV
Q = 6.14 MeV
40Ca (d, p)
• EXPT.
○ BEST ZS
△ BEST Z
— AV. Z
dσ/dω (PEAK) (mb/steradian)
Ed (MeV)
20
15
10
35
30
25
20
7
6
5
4
6
7
8
9
10
11
12
13

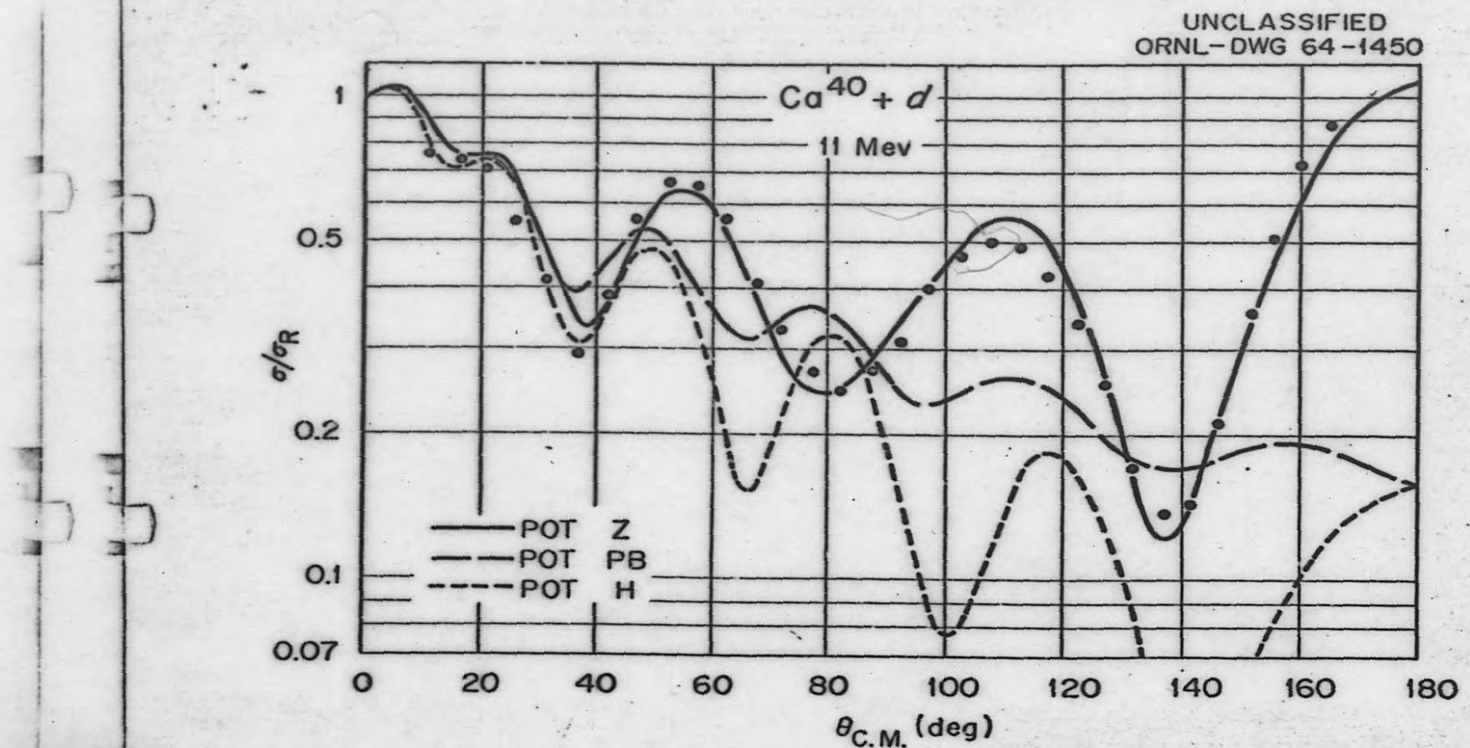
UNCLASSIFIED
ORNL-DWG 64-1450
$Ca^{40} + d$
11 Mev
1
0.5
0.2
0.1
0.07
σ/σ_R
POT Z
POT PB
POT H
0
20
40
60
80
100
120
140
160
180
$\theta_{C.M.}$ (deg)

Figure 13

Figure 14

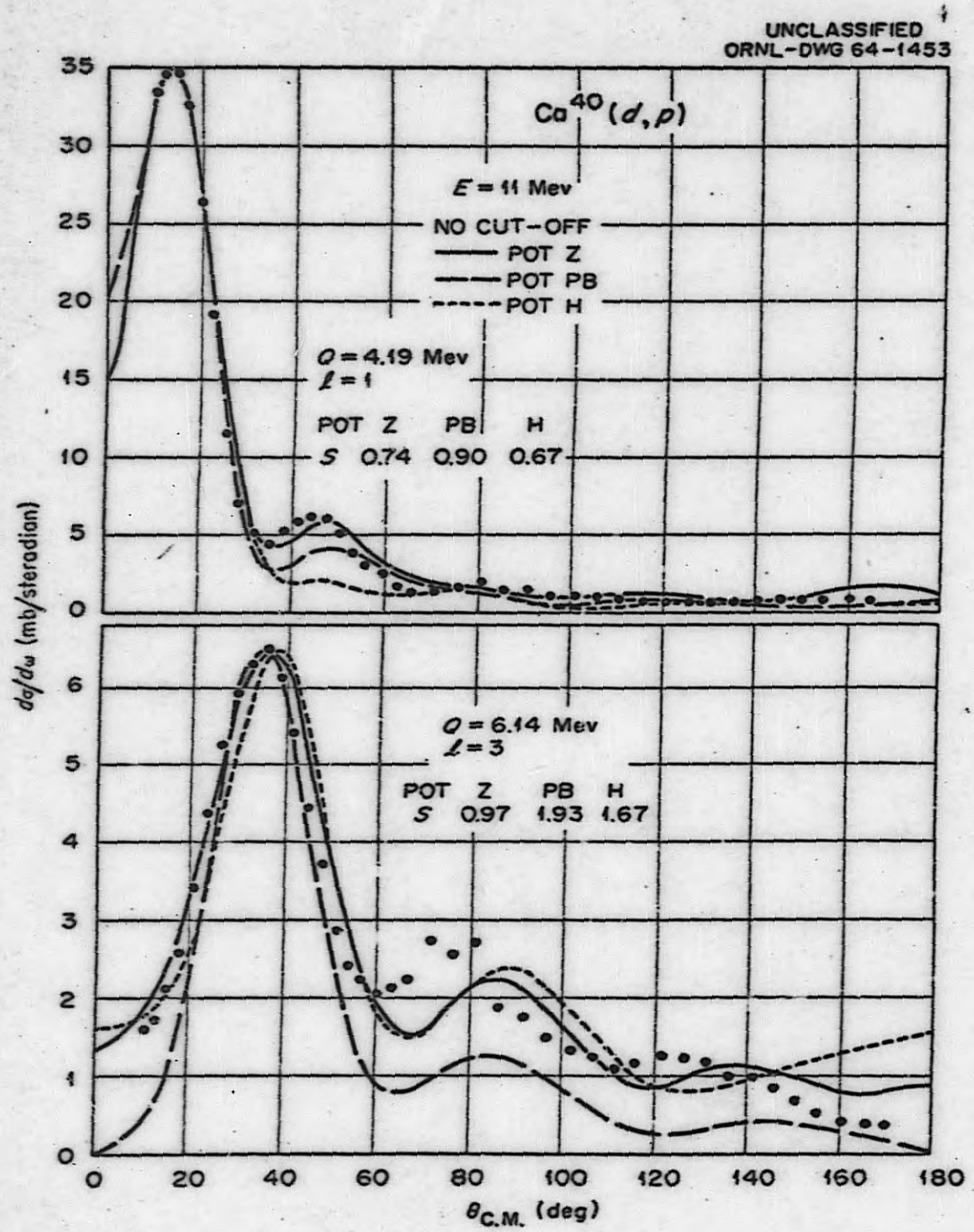
UNCLASSIFIED
ORNL-DWG 64-1453
$Ca^{40}(d,p)$
E = 11 Mev
NO CUT-OFF
POT Z
POT PB
POT H
Q = 4.19 Mev
ℓ = 1
POT Z PB H
S 0.74 0.90 0.67
Q = 6.14 Mev
ℓ = 3
POT Z PB H
S 0.97 1.93 1.67
dσ/dω (mb/steradian)
θC.M. (deg)
0 20 40 60 80 100 120 140 160 180
0 1 2 3 4 5 6 10 15 20 25 30 35

Figure 15

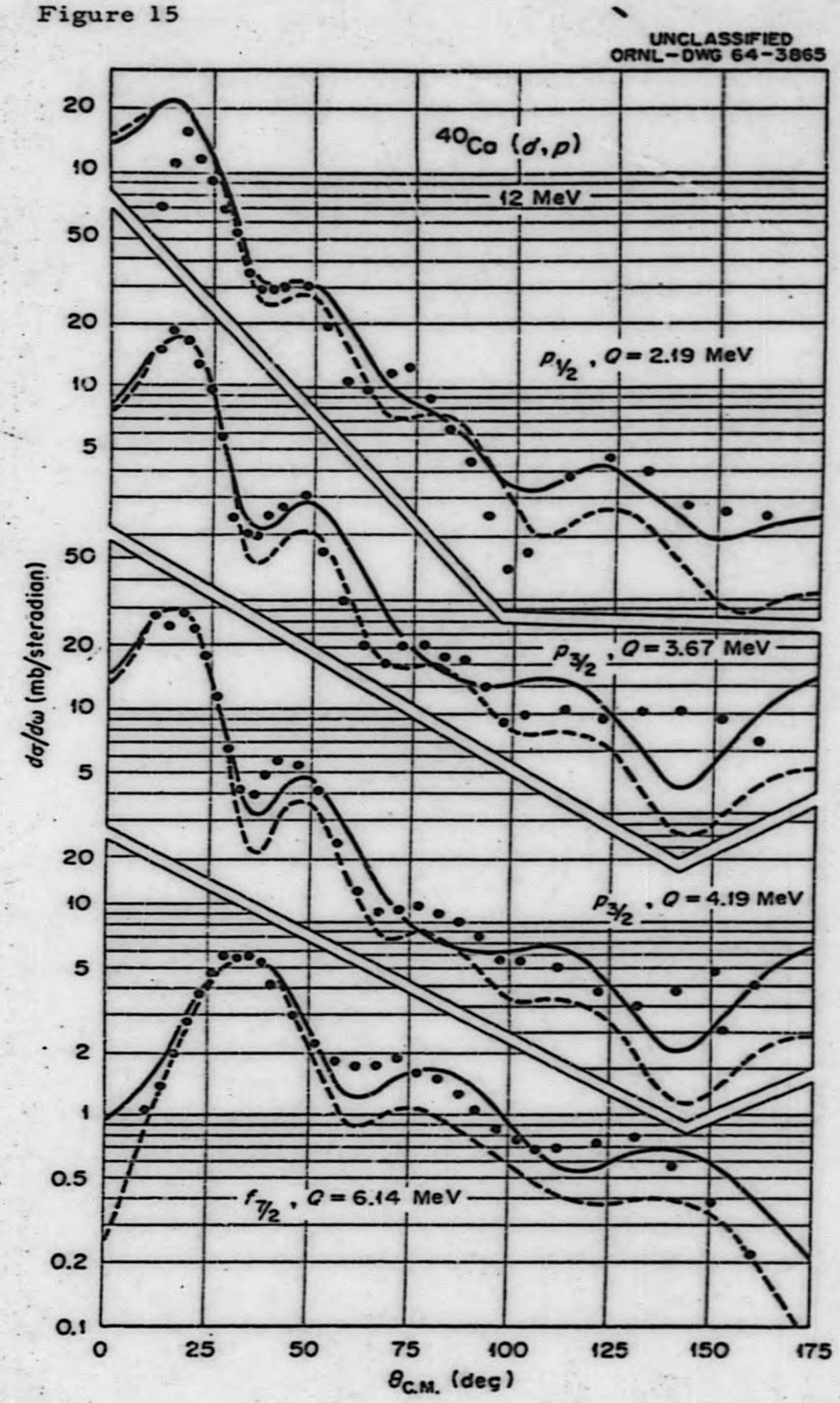
UNCLASSIFIED
ORNL-DWG 64-3865
^{40}Co (d, p)
12 MeV
$p_{1/2}$, Q = 2.19 MeV
$p_{3/2}$, Q = 3.67 MeV
$p_{3/2}$, Q = 4.19 MeV
$f_{7/2}$, Q = 6.14 MeV
dσ/dω (mb/steradian)
θC.M. (deg)
20
10
50
20
10
5
50
20
10
5
20
10
5
2
1
0.5
0.2
0.1
0
25
50
75
100
125
150
175

Figure 16

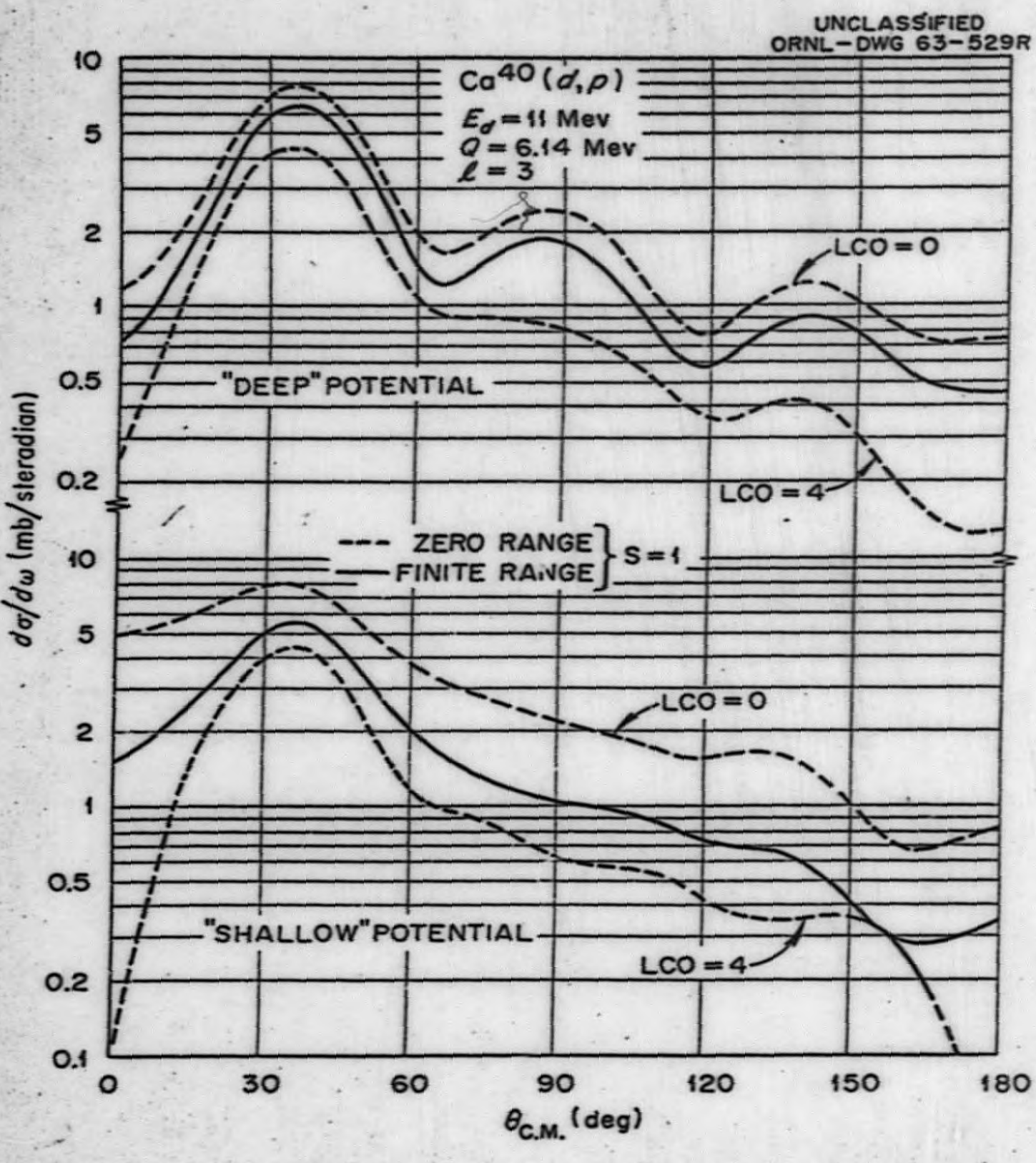
UNCLASSIFIED
ORNL-DWG 63-529R
$Ca^{40}(d,p)$
E_d = 11 Mev
Q = 6.14 Mev
ℓ = 3
LCO = 0
"DEEP" POTENTIAL
LCO = 4
ZERO RANGE
FINITE RANGE
S = 1
LCO = 0
"SHALLOW" POTENTIAL
LCO = 4
$d\sigma/d\omega$ (mb/steradian)
10
5
2
1
0.5
0.2
10
5
2
1
0.5
0.2
0.1
0
30
60
90
120
150
180
$\theta_{C.M.}$ (deg)

Figure 17

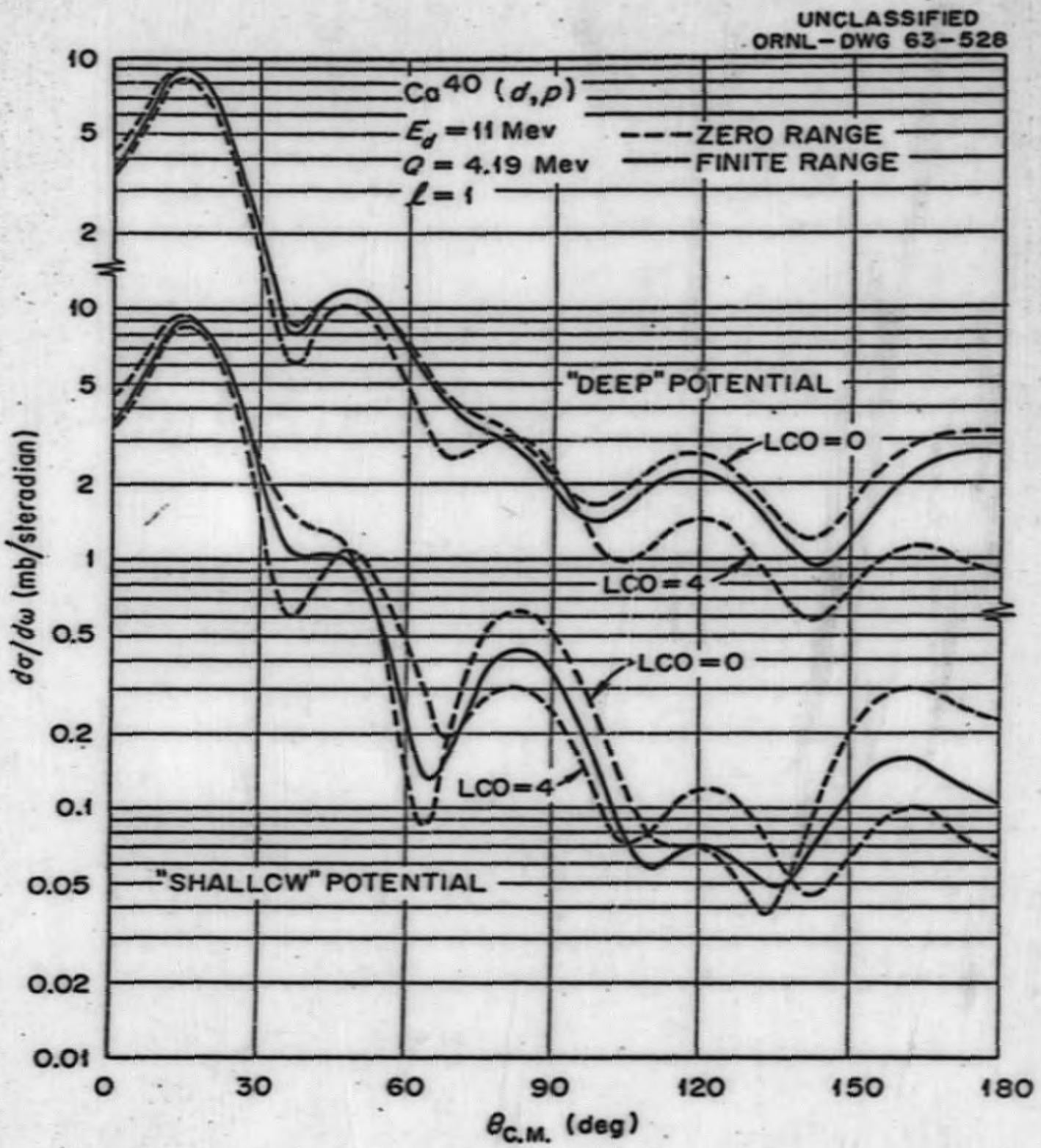
UNCLASSIFIED
ORNL-DWG 63-528
Ca40 (d,p)
Ed = 11 Mev
Q = 4.19 Mev
ℓ = 1
ZERO RANGE
FINITE RANGE
"DEEP" POTENTIAL
LCO = 0
LCO = 4
LCO = 0
LCO = 4
"SHALLOW" POTENTIAL
dσ/dω (mb/steradian)
θC.M. (deg)
10
5
2
10
5
2
1
0.5
0.2
0.1
0.05
0.02
0.01
0
30
60
90
120
150
180

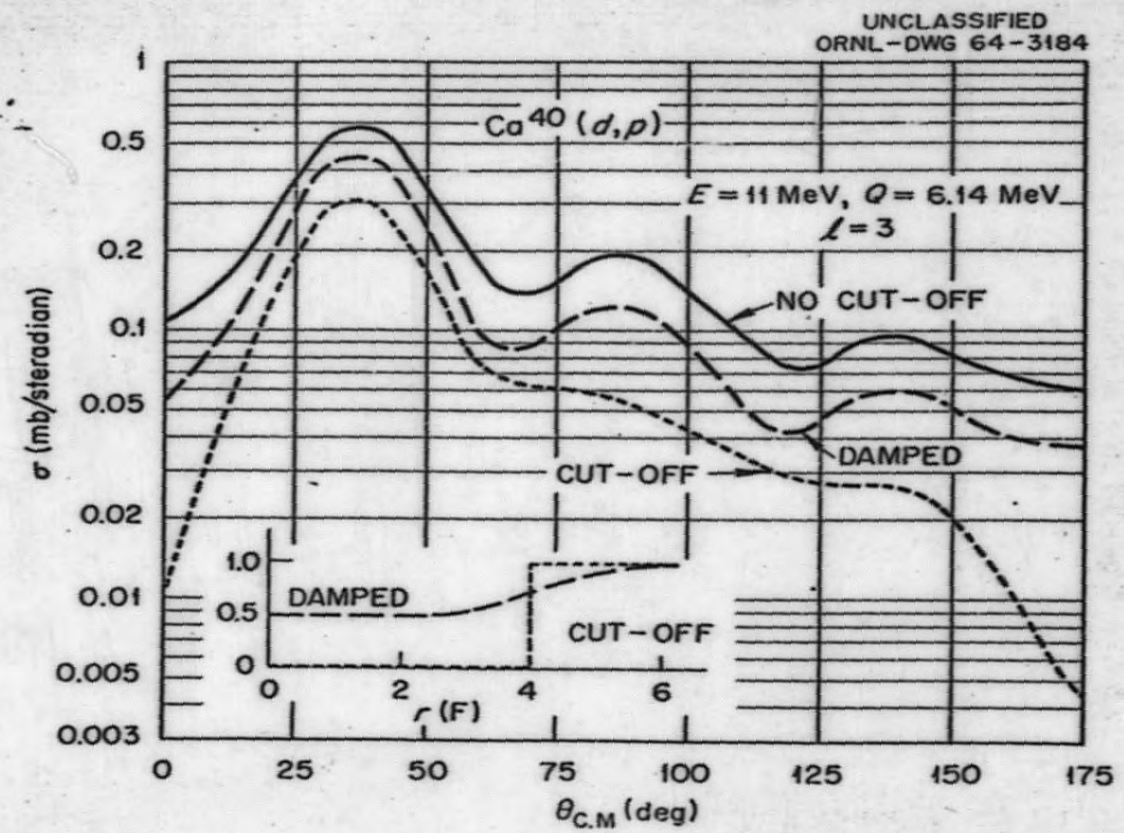
UNCLASSIFIED
ORNL-DWG 64-3184
Ca40 (d,p)
E = 11 MeV, Q = 6.14 MeV
ℓ = 3
NO CUT-OFF
DAMPED
CUT-OFF
σ (mb/steradian)
1
0.5
0.2
0.1
0.05
0.02
0.01
0.005
0.003
1.0
0.5
0
DAMPED
CUT-OFF
0
2
4
6
r (F)
0
25
50
75
100
125
150
175
θC.M (deg)

Figure 18

Figure 19

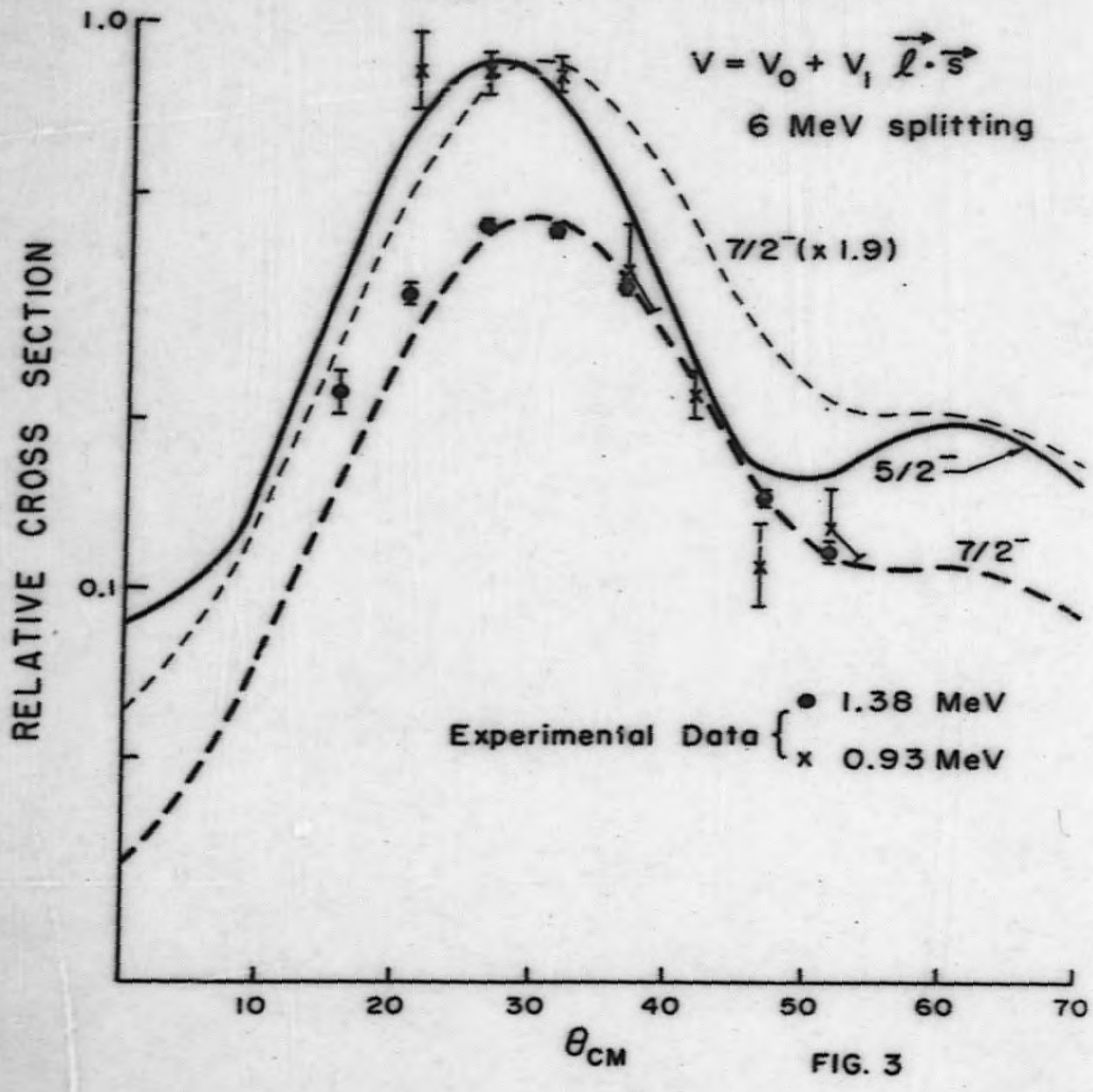

FIG. 3

Figure 20

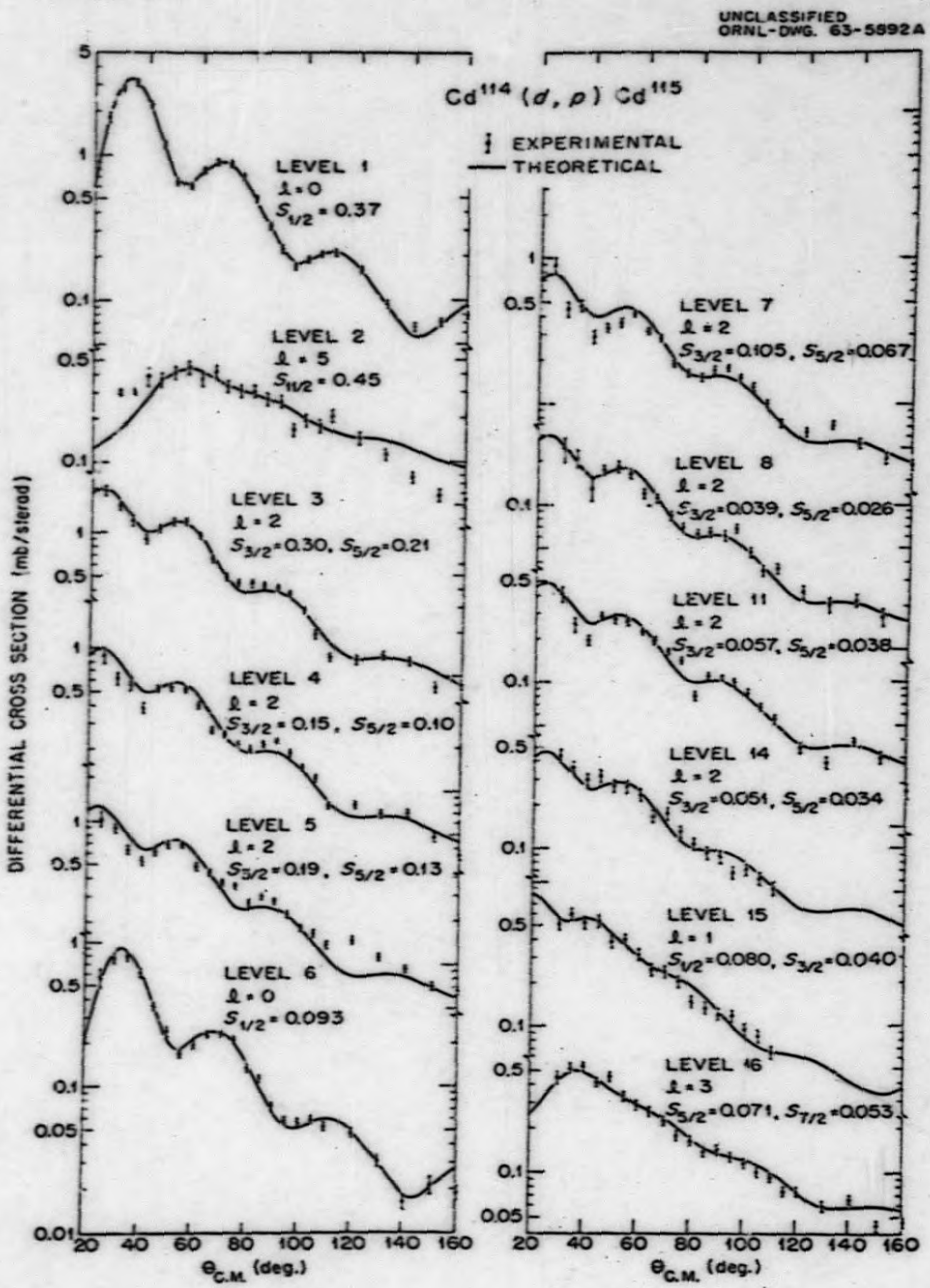
UNCLASSIFIED
ORNL-DWG. 63-5892A
Cd114 (d, p) Cd115
EXPERIMENTAL
THEORETICAL
LEVEL 1
ℓ = 0
S1/2 = 0.37
LEVEL 2
ℓ = 5
S11/2 = 0.45
LEVEL 3
ℓ = 2
S3/2 = 0.30, S5/2 = 0.21
LEVEL 4
ℓ = 2
S3/2 = 0.15, S5/2 = 0.10
LEVEL 5
ℓ = 2
S3/2 = 0.19, S5/2 = 0.13
LEVEL 6
ℓ = 0
S1/2 = 0.093
LEVEL 7
ℓ = 2
S3/2 = 0.105, S5/2 = 0.067
LEVEL 8
ℓ = 2
S3/2 = 0.039, S5/2 = 0.026
LEVEL 11
ℓ = 2
S3/2 = 0.057, S5/2 = 0.038
LEVEL 14
ℓ = 2
S3/2 = 0.051, S5/2 = 0.034
LEVEL 15
ℓ = 1
S1/2 = 0.080, S3/2 = 0.040
LEVEL 16
ℓ = 3
S5/2 = 0.071, S7/2 = 0.053
DIFFERENTIAL CROSS SECTION (mb/sterad)
θC.M. (deg.)
θC.M. (deg.)

Figure 21

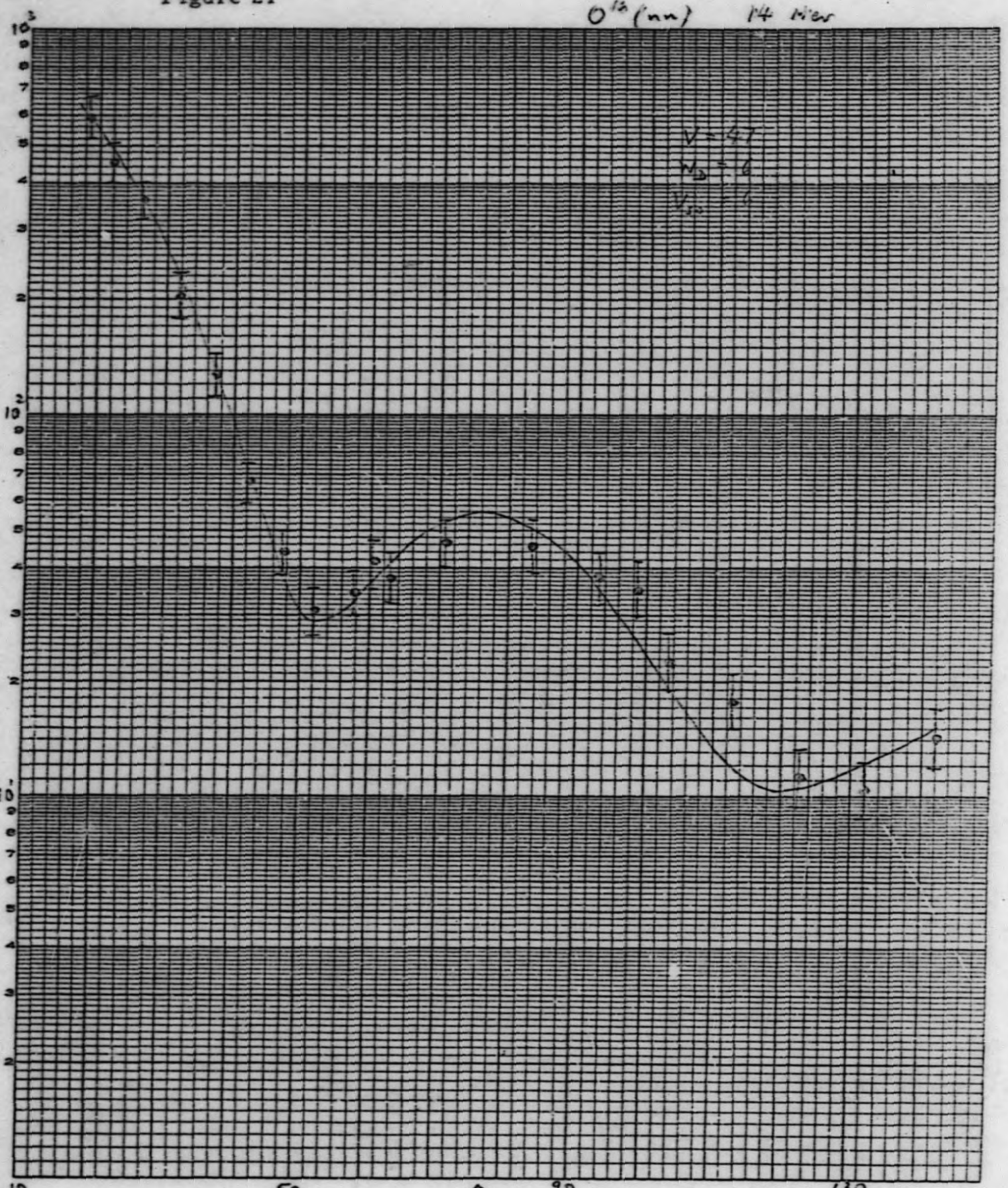

Figure 22

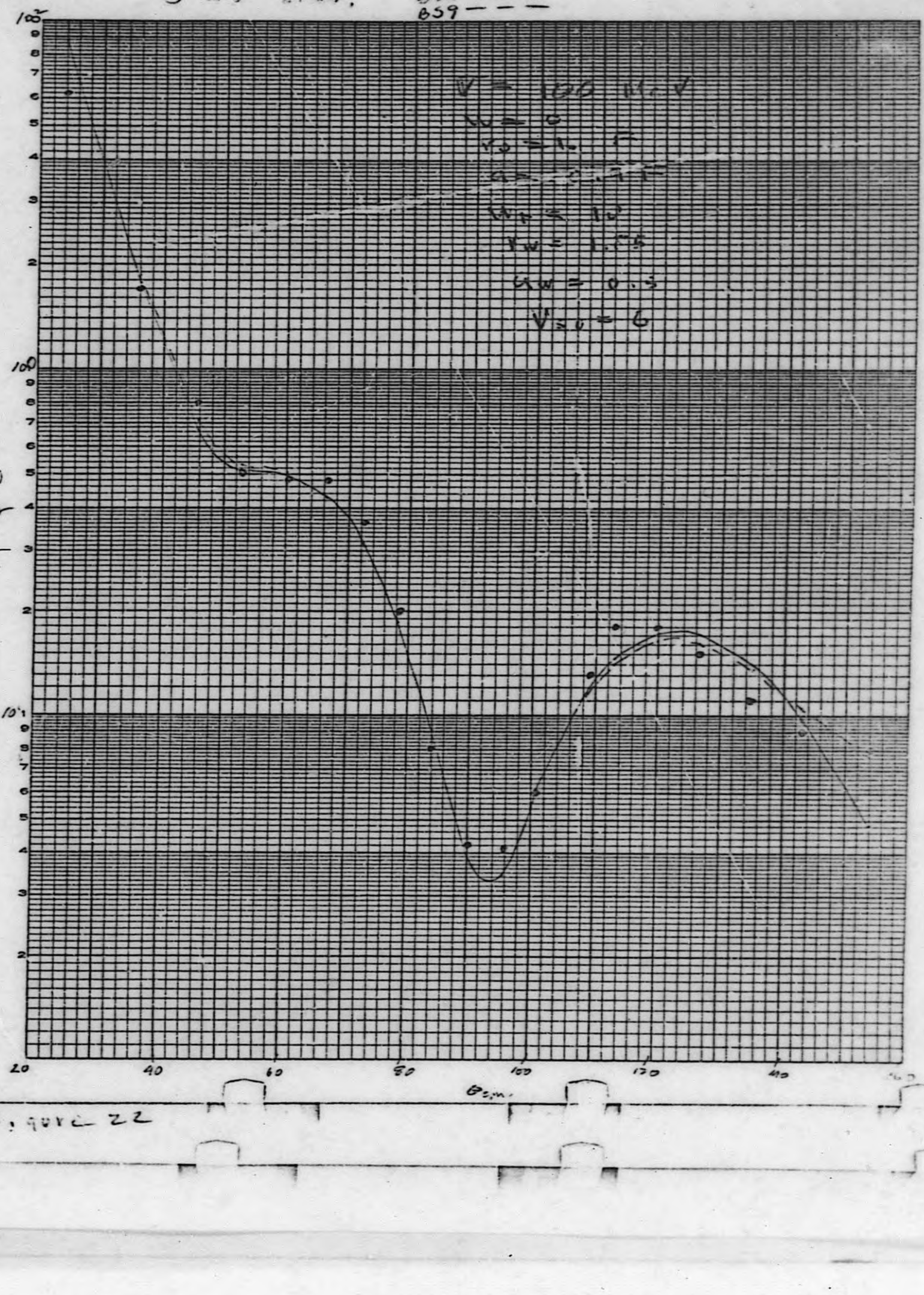

Figure 22

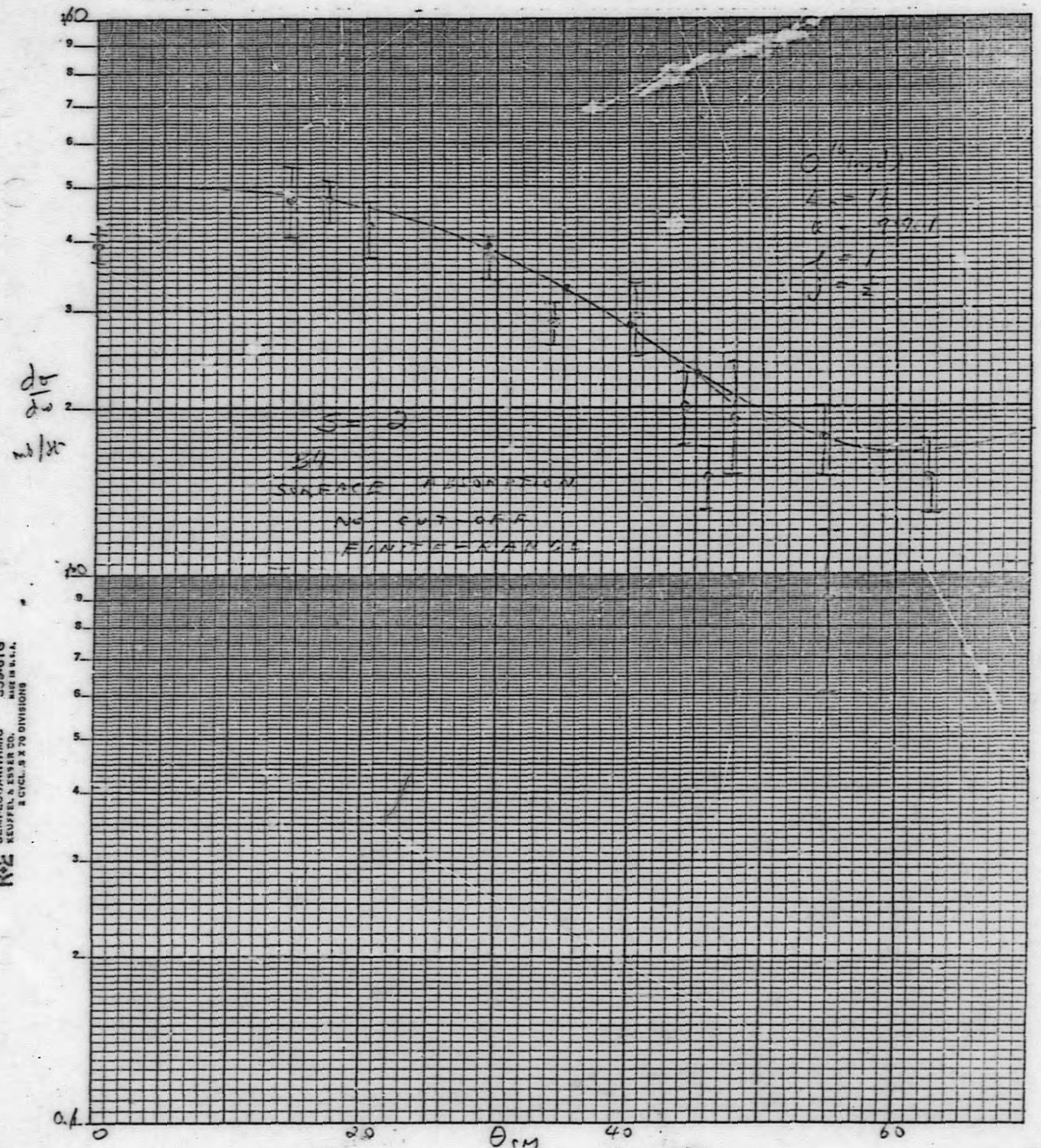
$\frac{dv}{d\omega}$
m/w
S = 2
SCIENCE ACCOMPTION
NO CUT-OFF
FINITE-AMPLITUDE
0.1
2
3
4
5
6
7
8
9
10
0
20
40
60
θ_{rM}
SEMI-LOGARITHMIC 359-61G
KEUFFEL & ESSER CO.
MADE IN U.S.A.
2 CYCL. 5 X 70 DIVISIONS

Figure 23

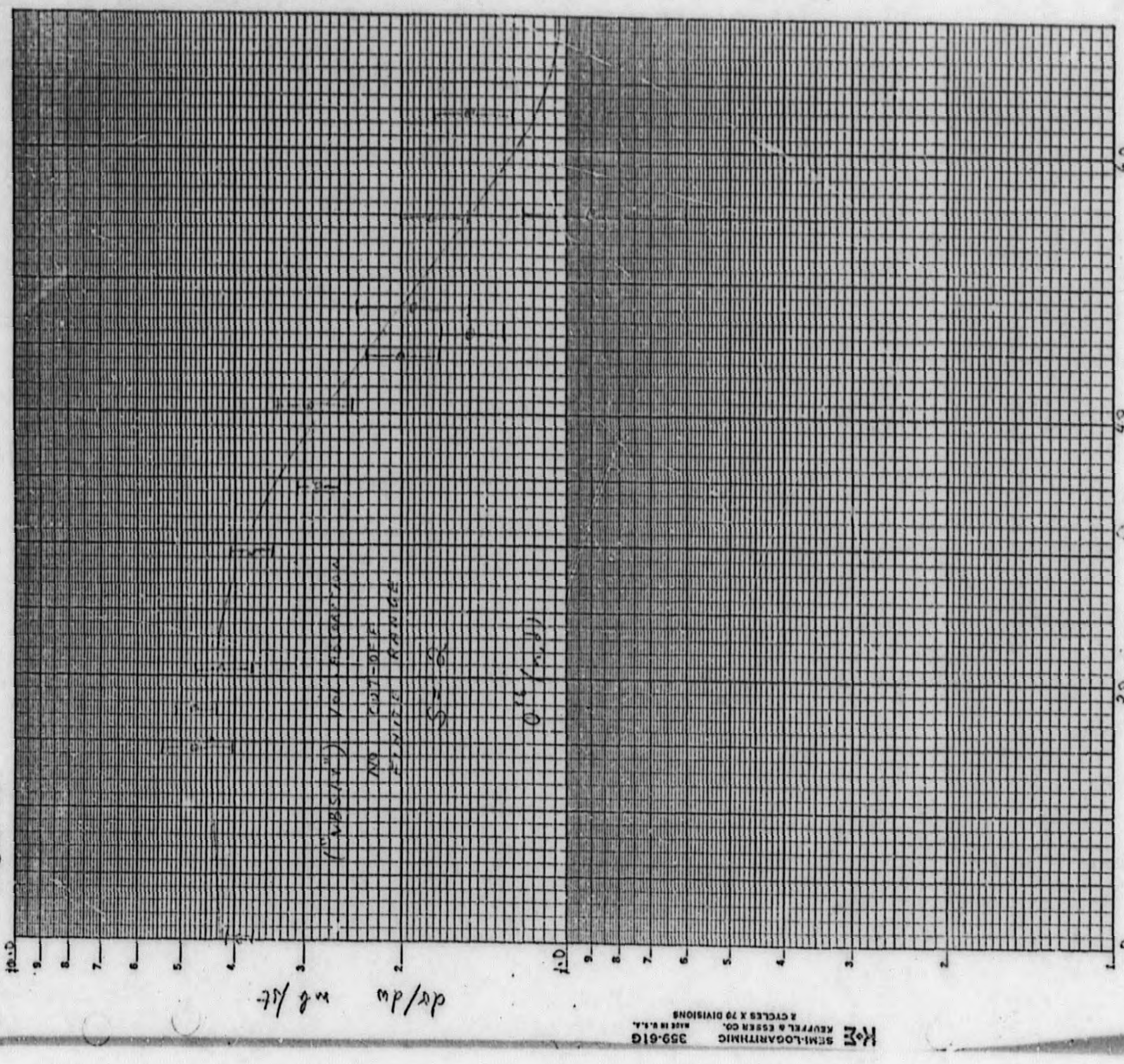

Figure 24

Figure 24

Figure 25

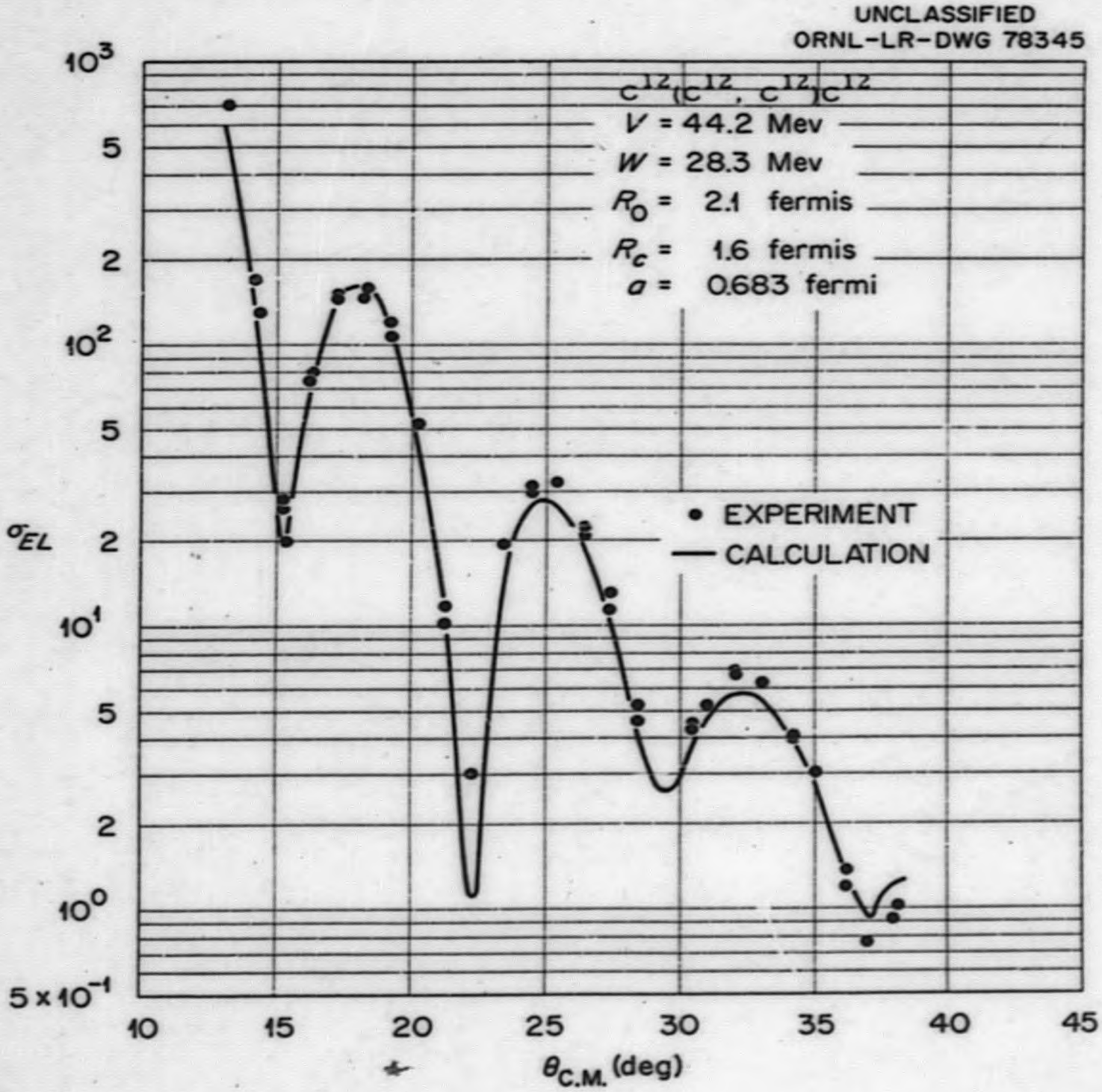
UNCLASSIFIED
ORNL-LR-DWG 78345
$C^{12}(C^{12}, C^{12})C^{12}$
V = 44.2 Mev
W = 28.3 Mev
R_0 = 2.1 fermis
R_c = 1.6 fermis
a = 0.683 fermi
• EXPERIMENT
— CALCULATION
σ_{EL}
10^3
5
2
10^2
5
2
10^1
5
2
10^0
5×10^{-1}
10
15
20
25
30
35
40
45
$\theta_{C.M.}$ (deg)

Figure 26

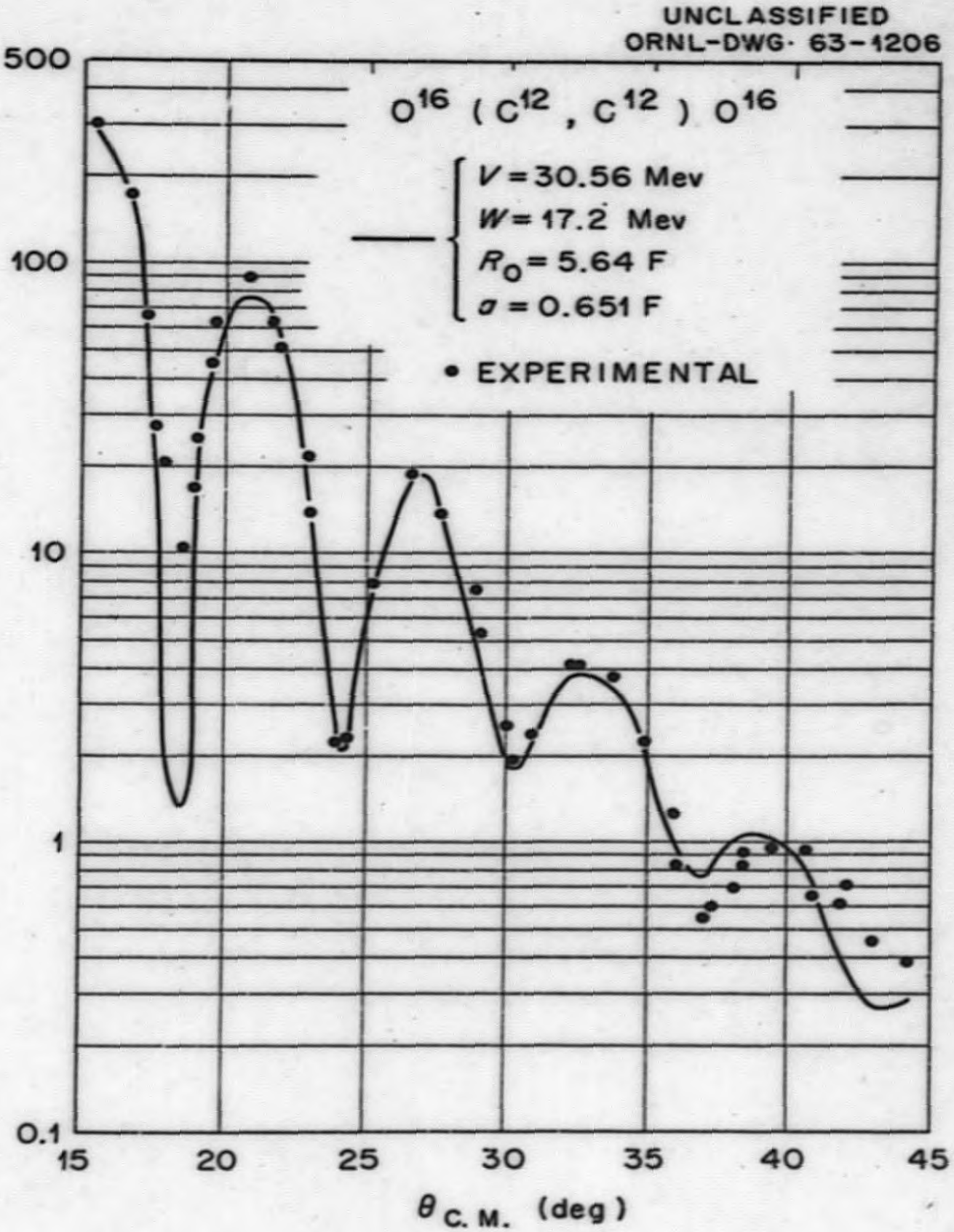
UNCLASSIFIED
ORNL-DWG· 63-1206
O^{16} (C^{12} , C^{12}) O^{16}
V = 30.56 Mev
W = 17.2 Mev
R_0 = 5.64 F
σ = 0.651 F
• EXPERIMENTAL
500
100
10
1
0.1
15
20
25
30
35
40
45
σ (θ) (mb/sr)
$\theta_{C.M.}$ (deg)

Figure 27

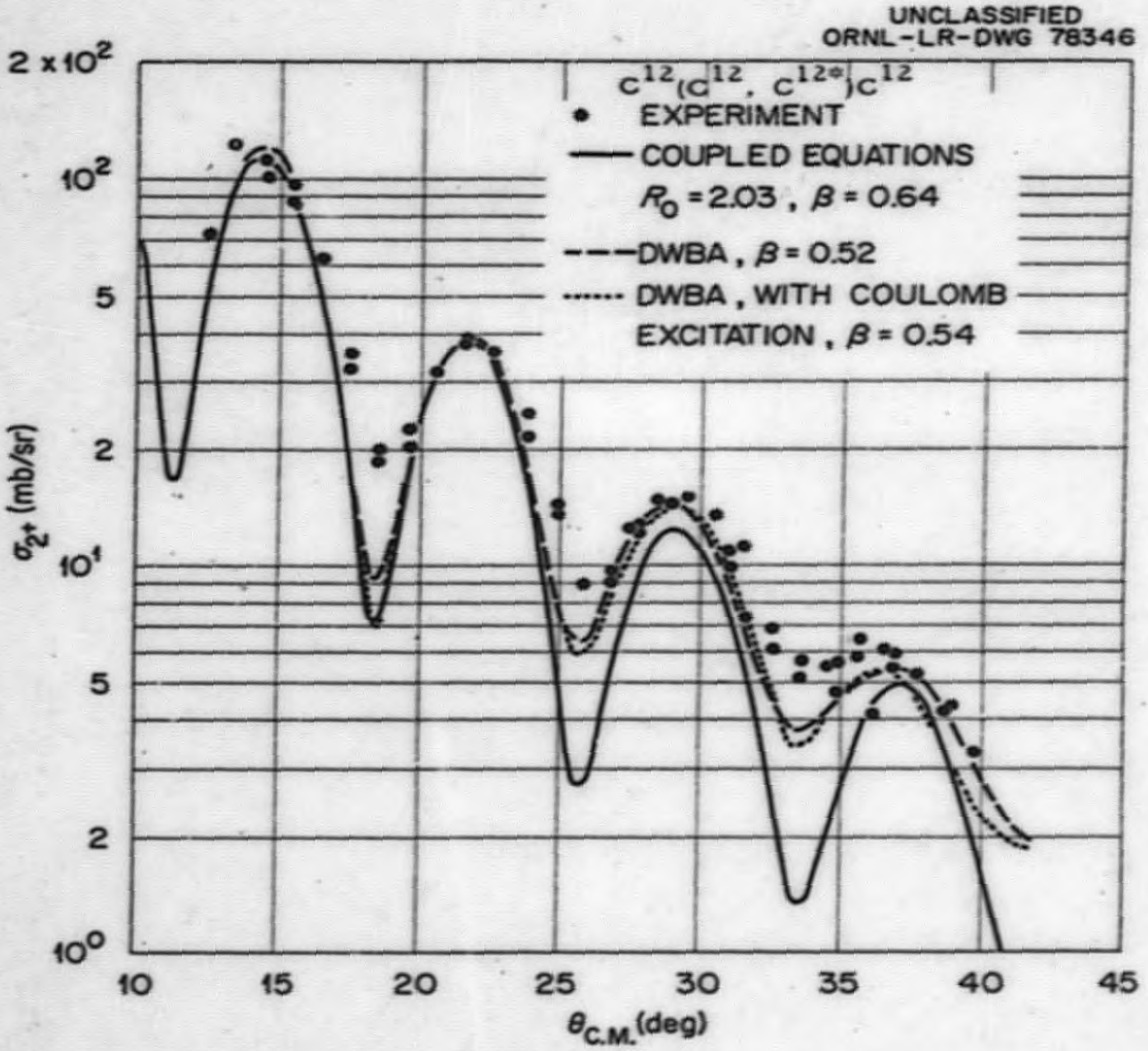
UNCLASSIFIED
ORNL-LR-DWG 78346
$C^{12}(C^{12}, C^{12*})C^{12}$
EXPERIMENT
COUPLED EQUATIONS
$R_0 = 2.03$, $\beta = 0.64$
DWBA , $\beta = 0.52$
DWBA , WITH COULOMB EXCITATION , $\beta = 0.54$
σ_{2^+} (mb/sr)
2×10^2
10^2
5
2
10^1
5
2
10^0
10
15
20
25
30
35
40
45
$\theta_{C.M.}$ (deg)

Figure 28

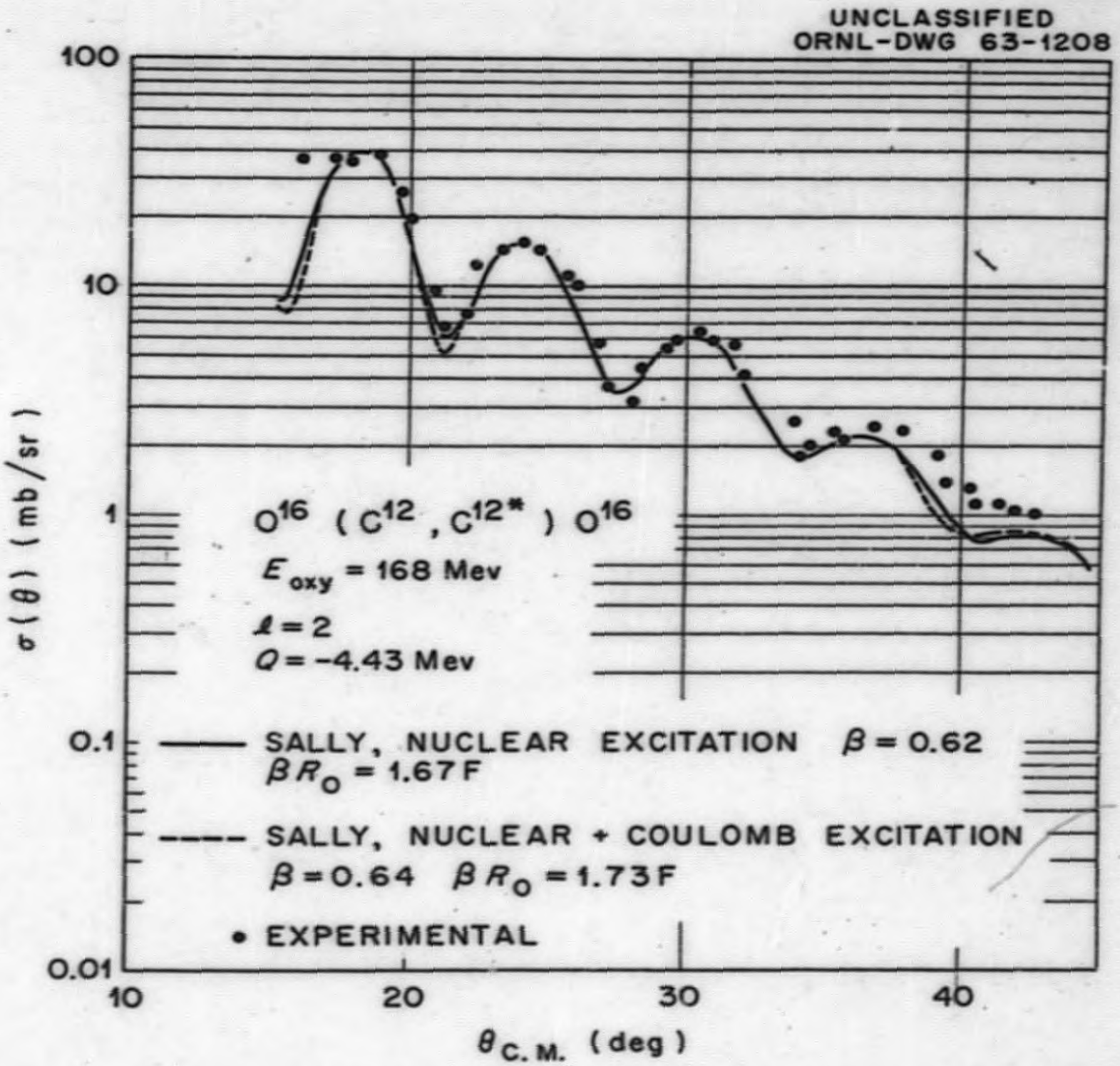
UNCLASSIFIED
ORNL-DWG 63-1208
100
10
1
0.1
0.01
10
20
30
40
σ(θ) (mb/sr)
θ C.M. (deg)
O16 (C12 , C12*) O16
E oxy = 168 Mev
ℓ = 2
Q = -4.43 Mev
SALLY, NUCLEAR EXCITATION β = 0.62
β R0 = 1.67 F
SALLY, NUCLEAR + COULOMB EXCITATION
β = 0.64 β R0 = 1.73 F
EXPERIMENTAL

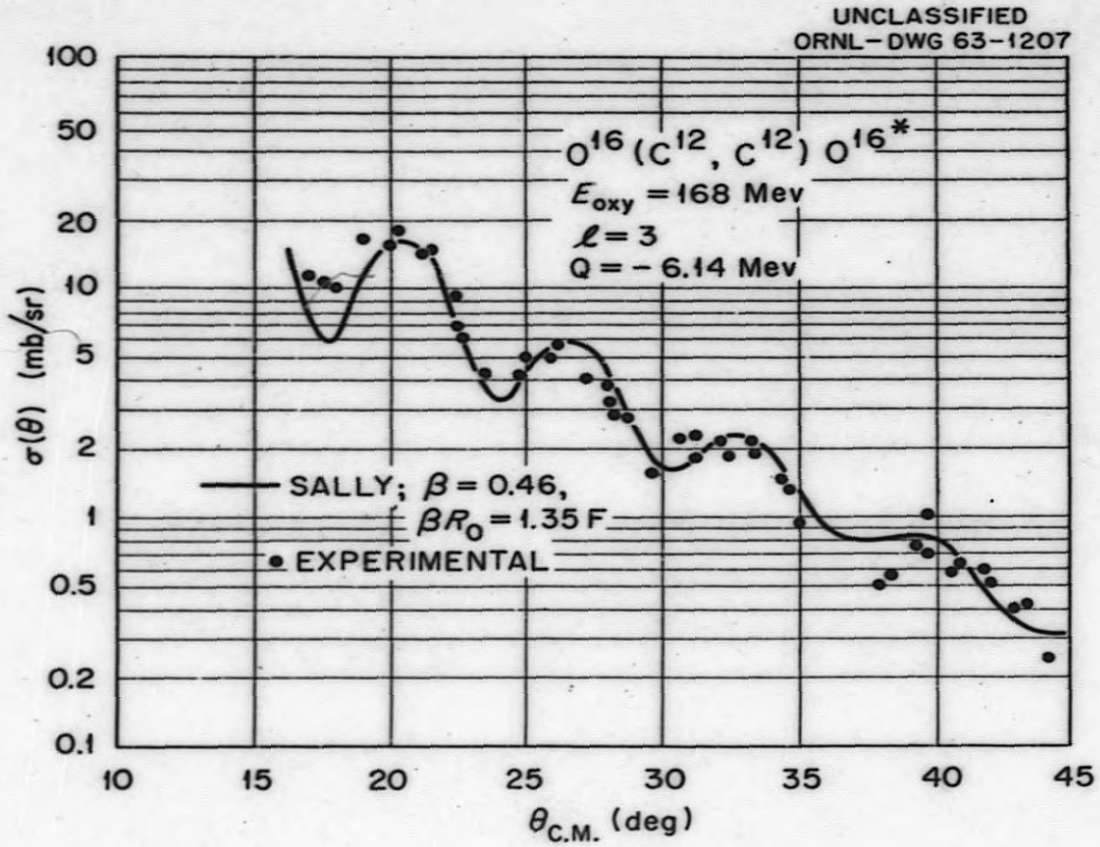

Figure 29

END